PRRIP DRAFT
Manuscript Development for Possible Publication in 2014

Directed Vegetation Research: Lateral Bar Erosion Study

Platte River, NE

33870001.00

Cardno ENTRIX
Shaping the Future

Document Information

Prepared for	Platte River Recovery Implementation Program
Project Name	Directed Vegetation Research, Platte River, NE
Project Number	33870001.00
Project Manager	Natasha Bankhead
Date	December 2012

Prepared for:

PLATTE RIVER
RECOVERY IMPLEMENTATION PROGRAM

Platte River Recovery Implementation Program
4111 4th Avenue, Suite 6
Kearney, NE 68845

Prepared by:

Cardno ENTRIX
Shaping the Future

Cardno ENTRIX
1223 Jackson Avenue East, Suite 301, Oxford, MS 38655

Executive Summary

Management of vegetation on bars along the Central Platte River continues to be an issue in terms of sediment dynamics, channel planform, and habitat availability for endangered bird species. Braided channels are characterized by abundant bedload and mobile bank/bar sediments with little if any cohesive strength. Removal of vegetation from bars and near-bank zones could alter the morphology of the Central Platte River by reducing the resistance of the bar and bank materials to hydraulic and geotechnical erosion, thus re-mobilizing bank and/or bar sediments, and increasing the sediment load within the system.

A previous study of vegetation removal mechanisms by Pollen-Bankhead et al. (2010) showed that drag forces alone only have the potential to remove the youngest and weakest cottonwood and sandbar willow seedlings; once either of these species, or *Phragmites* and Reed canarygrass are established. Removal of these plants through drag forces alone is very unlikely even during *Short Duration High Flow* events (SDHFs). In the same study, the potential for vertical scour around plant stems to increase the potential for plant removal during these SDHFs was also examined, but calculations suggested that this process was not significant enough to increase the likelihood of plant removal. The process of hydraulic erosion, undercutting and subsequent geotechnical failures at bar and bank edges was suggested as an alternative mechanism by which flowing water in the Central Platte may be able to remove bar vegetation.

In this study, therefore, Cardno ENTRIX was charged with assessing the effects of vegetation growth on bar and bank edge stability and erosion rates, and assessing the implications for PRRIPs Flow-Sediment-Mechanical (FSM) management strategy in the Central Platte River. To undertake this task, Cardno ENTRIX collected *in situ* field data to populate the mechanistic Bank Stability and Toe Erosion Model (BSTEM Dynamic Ver. 1.0) so that bar and bank erosion volumes, with and without vegetation, and under both low flow conditions and SDHF events, could be compared. Sub-objectives of the study included:

1. Quantification of resisting forces provided by bed and bank materials, with and without vegetation, for cottonwood seedlings up to 2-years-old, *Phragmites*, and Reed canarygrass.

2. Quantification of lateral erosion volumes at bank and bar edges, with and without vegetation, to include low flows, and a SDHF event up to 8,000 ft^3s^{-1}, using BSTEM Dynamic 1.0.

Modeling results showed that in general, cottonwood seedlings had the least effect on eroded volumes compared to the calibration run (5 % increase in eroded volume to a 36 % reduction). The Reed canarygrass runs had the most complex results because of the substantial reinforcement of the upper 0.5m layer, combined with a relatively shallow root zone that could be undercut by hydraulic scour (19 % increase in eroded volume to a 47.7 % reduction). In contrast, *Phragmites* had a dramatic effect on eroded volumes compared to the calibration runs (52% to 100 % reduction in eroded volume). In the model runs, lateral erosion of bar and bank edges effectively removed young cottonwood seedlings and areas of Reed canarygrass that could be undercut by hydraulic erosion. The model results for *Phragmites* , however, suggested that its deep rooting network is unlikely to be undercut and the root-reinforcement provided by the interconnected rhizome networks makes resistance to geotechnical failure high. Lateral erosion at bar and bank edges was therefore resisted in most cases by stands of *Phragmites* during both long duration lower flows, or during SDHF events.

The implication for management of cottonwood seedlings in the Central Platte River, is that little intervention to mechanically remove young cottonwoods should be required, especially at lower elevations. Because lateral erosion was still predicted in the all of the cottonwood model runs, even under the highest root densities modeled, it is likely that those cottonwoods that do survive on bars will be

located away from bar edges, and/or at elevations that are subject to shorter durations of hydraulic scour, so that roots have time to establish. Cottonwoods growing at higher bar elevations may, therefore, need to be removed mechanically if their roots become established.

For Reed canarygrass the management implications of the model results are that SDHFs should be capable of removing newly establishing stands with shallower root networks, or locations where the rooting depth to bar/bank height ratio is low. As with cottonwood seedlings, as the roots grow to form a denser, deeper mat, it will become increasingly difficult for flows of any magnitude to remove this species. This will be especially true on bars that are lower in height, where the rooting depth to bar/bank height ratio is high. Because Pollen-Bankhead et al. (2010) showed that Reed canarygrass is unlikely to be removed through drag forces acting on the stems, continued mechanical removal of this species may be necessary where undercutting, and resulting cantilever failures of root-reinforced blocks is unlikely.

In terms of vegetation management on channel bars, *Phragmites* poses more of a problem than cottonwood and Reed canarygrass. The model results presented in this study show that with *Phragmites*, little erosion, be it hydraulic or geotechnical, can occur once the rhizomes have grown throughout the depth of the bar or bank, even during SDHFs. The first directed vegetation study also showed that this species is very unlikely to be removed through drag forces acting on the stems, even during SDHFs. Mechanical removal of the above and below ground biomass of *Phragmites* is likely to be required to remove this species.

Table of Contents

Executive Summary ii

1 Introduction and Background 1-5
- 1.2 Problems and Objectives 1-7

2 Fundamentals of Bank Stability 2-8
- 2.2 The Dynamic Bank Stability and Toe Erosion Model (BSTEM-Dynamic) 2-11
  - 2.2.1 Assessing Geotechnical Failure 2-11
  - 2.2.2 Modeling Movement of the Groundwater Table 2-11
  - 2.2.3 Assessing Hydraulic Erosion 2-12
  - 2.2.4 Root Reinforcement by Riparian Vegetation 2-14

3 Field Data Collection 3-16
- 3.1 *In Situ* Field Data Collection and Material Properties 3-17
  - 3.1.1 Quantifying Geotechnical Resistance to Failure 3-17
  - 3.1.2 Quantifying Hydraulic Resistance to Failure 3-20
  - 3.1.3 Reinforcement due to Vegetation Roots 3-22

4 BSTEM Dynamic Runs 4-23
- 4.1 Flow Data and Modeling Locations 4-23
- 4.2 Calibration of BSTEM Dynamic 1.0 using May 2011 and August 2011 cross sections 4-25
- 4.3 Vegetation Input parameters for BSTEM 4-27
  - 4.3.1 Measured Root and Stem Properties to account for effects of roots on critical shear stress. 4-27
  - 4.3.2 Vegetation input parameters for runs with vegetation 4-28
- 4.4 BSTEM Dynamic Model Results with Vegetation 4-29
  - 4.4.2 Cottonwood 4-31
  - 4.4.3 Reed canarygrass 4-35
  - 4.4.4 Phragmites 4-39
- 4.5 Effects of low flows and SDHFs on timing and magnitudes of geotechnical and hydraulic erosion at bank and bar edges 4-44
  - 4.5.2 BSTEM results for a 3-day SDHF event of 8,000 ft^3/s 4-47

5 Implications for Vegetation Management and Sediment Dynamics in the Central Platte River 5-48
- 5.1 Cottonwood seedlings 5-48
- 5.2 Reed canarygrass 5-49
- 5.3 *Phragmites* 5-49
- 5.4 Rates of lateral erosion compared to total channel width, and implications for vegetation management 5-50

6 Summary and Conclusions 6-51

7 References 7-53

Table of Figures

Figure 1-1 PRRIP historical cross-section locations, with cross sections investigated in this study shown in red. 1-6
Figure 2-1 Conceptual model of bank and bar edge retreat that stresses the importance of the interaction of hydraulic forces that cause steepening of the lower part of the face, resulting in failure of the bank mass. 2-10
Figure 2-2 Segmentation of local flow areas and hydraulic radii. 2-14
Figure 3-1 Sampling locations within each cross section. Water levels during field investigations were lower than those seen in the aerial photograph taken from Google Earth. In addition, with the very dynamic nature of the bars in this reach, "bar edges" identified during fieldwork may be shown as "bar" locations in these photos. 3-16
Figure 3-2 Left: Humboldt Torvane used to define material shearing resistance. Right: Pocket Penetrometer used to determine unconfined material compressive shear strength. 3-18
Figure 3-3 Histogram of cohesion values calculated from Torevane data collected *in situ*. 3-18
Figure 3-4 Shields diagram for incipient motion (modified from Buffington, 1999). The y-axis is defined by $\tau_o = \gamma RS$ where τ_o is the mean bed shear stress, in N/m^2 (Pa) and R is the hydraulic radius, in meters and the x-axis is defined by $\tau_o = \tau_{og} + \tau_{of} + \tau_{ov}$ where the subscripts *g*, *f* and *v* signify the grain, form and vegetal components of the boundary shear stress, respectively 3-20
Figure 3-5 Histogram showing the distribution of d_{50} values in the bank and bar samples taken at XS2, XS13, and XS20. 3-21
Figure 4-1 Flow data at the USGS gage 06768000 Platte River near Overton, NE for the calibration and modeling period May 1st to August 31st 2011, used as input for BSTEM-Dynamic. 4-23
Figure 4-2 Calibration runs compared to measured May 2011 to August 2011 cross sections. 4-26
Figure 4-3 Before and after bar- and bank- edge profiles from BSTEM Dynamic runs compared to the calibration runs at a) XS2-3 and b) XS2-6 with cottonwood seedlings. 4-32
Figure 4-4 Before and after bar- and bank- edge profiles from BSTEM Dynamic runs compared to the calibration runs at a) XS13-2 and b) XS13-6 with cottonwood seedlings. 4-33
Figure 4-5 Before and after bar- and bank- edge profiles from BSTEM Dynamic runs compared to the calibration runs at a) XS20-6 and b) XS20-7 with cottonwood seedlings. 4-34
Figure 4-6 Before and after bar- and bank- edge profiles from BSTEM Dynamic runs compared to the calibration runs at a) XS2-3 and b) XS2-6 with Reed canarygrass. 4-36
Figure 4-7 Before and after bar- and bank- edge profiles from BSTEM Dynamic runs compared to the calibration runs at a) XS13-2 and b) XS13-6 with Reed canarygrass. 4-37
Figure 4-8 Before and after bar- and bank- edge profiles from BSTEM Dynamic runs compared to the calibration runs at a) XS20-6 and b) XS20-7 with Reed canarygrass. 4-38
Figure 4-9 Before and after bar- and bank- edge profiles from BSTEM Dynamic runs compared to the calibration runs at a) XS2-3 and b) XS2-6 with *Phragmites*. 4-40
Figure 4-10 Before and after bar- and bank- edge profiles from BSTEM Dynamic runs compared to the calibration runs at a) XS13-2 and b) XS13-6 with *Phragmites*. 4-41
Figure 4-11 Before and after bar- and bank- edge profiles from BSTEM Dynamic runs compared to the calibration runs at a) XS20-6 and b) XS20-7 with *Phragmites*. 4-42
Figure 4-12 Illustration of how rooting depth and density affect extent of undercutting and resulting geotechnical failures. 4-43
Figure 4-13 Timing and magnitude of hydraulic and geotechnical erosion over the period modeled in BSTEM, for CW1 and CW2 scenarios. 4-44
Figure 4-14 Timing and magnitude of hydraulic and geotechnical erosion over the period modeled in BSTEM, for RCG scenarios. 4-45
Figure 4-15 Timing and magnitude of hydraulic and geotechnical erosion over the period modeled in BSTEM, for *Phragmites* scenarios. 4-46
Figure 4-16 Volumes of hydraulic versus geotechnical erosion in each model run. 4-46

Table of Tables

Table 3-1 Field data collected in situ to measure shear strength of the bar and bank edges 3-19
Table 3-2 Particle size d_{50} from samples taken at the three cross sections studied, and corresponding τ_c values to be used in BSTEM Dynamic 1.0, calculated using the Shields entrainment curve (1936). 3-21
Table 3-3 Maximum root densities measured in the Central Platte for the species of interest in this study. 3-22
Table 4-1 Locations within each cross section selected for further BSTEM analysis. 4-24
Table 4-2 Values of measured versus modeled eroded volumes from May 2011 to Aug 2011 at the study locations. 4-25
Table 4-3 Factor increase in Tc values to account for variations in rooting densities for each set of vegetation runs in BSTEM Dynamic. 4-27
Table 4-4 Modified input parameters for BSTEM to account for root-reinforcement due to vegetation and increased critical shear stress values due to the presence of roots. 4-28
Table 4-5 Values of modeled eroded volumes, per meter of bar/bank edge, from May 2011 to Aug 2011 at the study locations, under various vegetation scenarios. Red numbers indicate model runs where more erosion was predicted compared to the calibration run. 4-30

This Page Intentionally Left Blank

1 Introduction and Background

The establishment of vegetation on bars, and the presence of a riparian corridor dominated by established cottonwood forests have produced a change in the relative resisting forces of the bed, banks and bar edges, compared to when the Platte River freely braided across its floodplain. The root networks of plants add resistance to the materials they grow in, affecting both the geotechnical resistance of bank and bar edges to mass-wasting processes (Simon and Collison, 2002; Pollen-Bankhead and Simon,2009; 2010), and also the resistance of bank and bar materials to hydraulic erosion from flow in the channel (Simon et al., 2011). The above-ground biomass of riparian plants serves to reduce the effective stress acting on grains making them less susceptible to hydraulic erosion. In materials that have lower cohesions (such as the sands that dominate the Platte River system), the addition of roots can have a particularly significant effect on the balance between resisting and driving forces acting on the bed and banks. For sand, typically having < 1 kPa of effective cohesion, even the addition of a few sparse cottonwood seedlings provide additional root-cohesion of roughly 3 kPa (BSTEM; Simon et al., 2011) that would increase the geotechnical resistance of the bar or bank material by ~300 %. In turn, this can lead to preferential erosion of the bed compared to root-reinforced bars and banks, and a produce a positive feedback that promotes development of a single rather than multiple thread river.

Plant roots can also have a significant influence on the resistance of streambank and bar materials to hydraulic scour. In recent years, a significant amount of work has been conducted on the hydraulic effects of vegetation on geomorphic processes. Several laboratory flume and field studies have examined the effects of plant roots on erosion in upland concentrated flows (Mamo and Bubenzer, 2001a; 2001b; Gyssels and Poesen, 2003; Gyssels *et al*., 2005; De Baets *et al*., 2006; 2007; Simon et al., 2011), and have shown an exponential decline in rill erodibility and soil detachment rates with increasing root-length densities and root biomass. Flume studies have shown that root architecture can play an important role in reducing soil erosion, with fine-rooted grasses being particularly effective at preventing soil detachment (De Baets *et al*., 2006). The results of these studies are also relevant for streambanks and bars with exposed root zones near the water surface because the root zone of vegetation growing on the top of streambanks and bars, rather than the plant canopy, interacts with flowing water.

Braided channels are characterized by abundant bedload and mobile bank/bar sediments with little if any cohesive strength. Removal of vegetation from bars and near-bank zones could alter the morphology of the Central Platte River by reducing the resistance of the bar and bank materials to hydraulic and geotechnical erosion, thus re-mobilizing bank and/or bar sediments, and increasing the sediment load of the system. The previous study of vegetation removal mechanisms by Pollen-Bankhead et al. (2010) showed that drag forces alone have only the potential to remove the youngest and weakest cottonwood and sandbar willow seedlings; once either of these species, or *Phragmites* and Reed canarygrass are established. Removal of these plants through drag forces alone is very unlikely even during *Short Duration High Flow* events (SDHFs; flow of 5,000 to 8,000 ft^3/s for three days). In the same study, the potential for vertical scour around plant stems to increase the potential for plant removal during these SDHFs was also examined, but calculations suggested that this process was not significant enough to increase the likelihood of plant removal. The authors concluded that the effects of vegetation on lateral erosion of bar and bank materials should also be investigated to examine:

1. The potential for SDHFs to remove bar and bank vegetation through the mechanisms of lateral hydraulic erosion of bank and bar edges, followed by subsequent geotechnical erosion of these surfaces, and
2. The volume of sediment eroded by SDHF events with and without bar and bank vegetation being present.

Three of The Platte River Recovery Implementation Program's (PRRIP) 22 monumented cross sections within the Elm Creek Reach were chosen for this study (Figure 1-1). These sites were selected based on:

1. The availability of repeat survey data for model calibration of the Bank-Stability and Toe-Erosion Model, (BSTEM) between two known periods in the;
2. Good site access for the field crew, and
3. The presence of mobile-bar edges that could be modelled with and without vegetation.

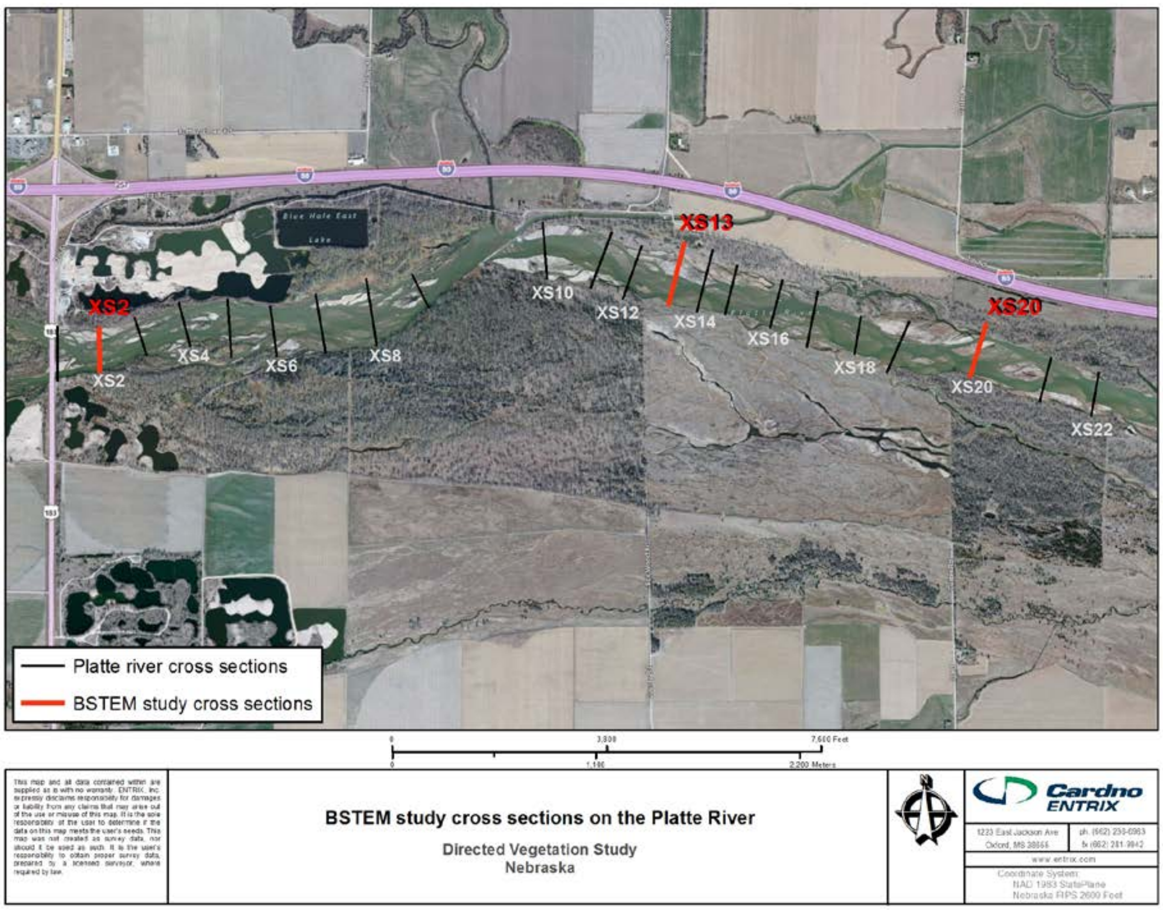

Figure 1-1 PRRIP historical cross-section locations, with cross sections investigated in this study shown in red.

1.2 Problems and Objectives

In this study, Cardno ENTRIX was charged with assessing the effects of vegetation growth on bar and bank edge stability and erosion, and assessing the implications for PRRIPs Flow-Sediment-Mechanical (FSM) management strategy in the Central Platte River. To undertake this task, Cardno ENTRIX collected *in situ* field data to populate the mechanistic Bank Stability and Toe Erosion Model (BSTEM Dynamic Ver. 1.0) so that bar and bank erosion volumes, with and without vegetation, and under both low flow conditions and SDHF events, could be compared. Sub-objectives of the study included:

3. Quantification of resisting forces provided by bed and bank materials, with and without vegetation, for cottonwood seedlings up to 2-years-old, *Phragmites*, and Reed canarygrass.

4. Quantification of lateral erosion volumes at bank and bar edges, with and without vegetation, to include low flows, and a SDHF event up to 8,000 ft^3s^{-1}, using BSTEM Dynamic 1.0.

2 Fundamentals of Bank Stability

Conceptual models of bank retreat and the delivery of bank sediment to the flow, emphasize the importance of interactions between hydraulic forces acting at the bed and bank toe, and gravitational forces acting on *in situ* bank materials (Carson and Kirkby, 1972; Thorne, 1982; Simon *et al*., 1991). Failure occurs when erosion of the bank toe and possibly the channel bed adjacent to the bank, increase the height and angle of the bank to the point that gravitational forces exceed the shear strength of the bank material. After failure, failed bank materials may be delivered directly to the flow and deposited as bed material, dispersed as wash load, or deposited along the toe of the bank as intact blocks, or as smaller, dispersed aggregates (Simon *et al*., 1991) (Figure 2-1). Whether these banks are at the edge of the channel, or at a bar edge, the physical processes remain the same. Any theory applied to hydraulic erodibility or geotechnical stability of "streambanks" can, therefore, also be applied to the edges of bars within the channel.

Bank materials do not maintain constant shear strength (resistance to mass failure) throughout the year. Strength varies with the pore-water pressure of the bank and as a function of the elevation of the saturated zone in the bank mass. The wetter the bank and the higher the water table, the weaker the bank mass becomes because of a loss of frictional strength, and the more prone it is to failure. Bank failures, however, do not occur frequently during high flows because the water in the channel is providing a buttressing, or confining force to the bank mass. This is true even though it is during high-flow events that the bank may be undercut by hydraulic forces. It is upon recession of the flow when the bank loses the confining force but still maintains a high degree of saturation when it is most likely to fail. This is why changes in flow regime can be very important in determining trends of bank stability over time.

Analyzing streambank stability is a matter of characterizing the gravitational forces acting on the bank and the geotechnical strength of the *in situ* bank material. Field data are required to quantify those parameters controlling this balance between force and resistance. If we initially envision a channel deepened by bed degradation or steepened by hydraulic forces in which the streambanks have not yet begun to fail, the gravitational force acting on the bank cannot overcome the resistance (shear strength) of the *in situ* bank material. Shear strength is a combination of frictional forces represented by the angle of internal friction (ϕ'), and effective cohesion (c'). Pore-water pressures in the bank serve to reduce the frictional component of shear strength. A factor of safety (F_s) is expressed then as the ratio between the resisting and driving forces. A value of unity (or the critical case) indicates the driving forces are equal to the resisting forces and that failure is imminent. The forces resisting failure on the saturated part of the failure surface are defined by the Mohr-Coulomb equation:

$$S_r = c' + (\sigma - \mu) \tan \phi' \qquad (1)$$

where μ is the pore pressure and ϕ' is the angle of internal friction.

The geotechnical driving force is given by the term:

$$F = W \sin\beta \qquad (2)$$

where, F = driving force acting on bank material (N), W = weight of failure block (N), and β = angle of the failure plane (degrees).

In the part of the streambank above the "normal" level of the groundwater table, bank materials are unsaturated, pores are filled with water and with air, and pore-water pressure is negative. The difference (μ_a - μ_w) between the air pressure (μ_a) and the water pressure in the pores (μ_w) represents matric-suction (ψ). This force acts to increase the shear strength of the material and with effective cohesion produces apparent cohesion (c_a). The increase in shear strength due to an increase in matric suction is described by the angle ϕ^b. This effect has been incorporated into the standard Mohr-Coulomb equation normally used for saturated soils by Fredlund *et al*. (1978), with a maximum value of

ϕ' under saturated conditions (Fredlund and Rahardjo, 1993). The effect of matric suction on shear strength is reflected in the apparent or total cohesion (c_a) term:

$$c_a = c' + (\mu_a - \mu_w) \tan \phi^b = c' + \psi \tan \phi^b \qquad (3)$$

As can be seen from equation 1, negative pore-water pressures (positive matric suction; ψ) in the unsaturated zone provide for cohesion greater than the effective cohesion, and thus, greater shearing resistance. This is often manifest in steeper bank slopes than would be indicated by ϕ'.

Thus, for the unsaturated part of the failure surface the resisting forces as modified by Fredlund *et al.* (1978) are used:

$$S_r = c' + (\sigma - \mu_a) \tan \phi' + (\mu_a - \mu_w) \tan \phi^b \qquad (4)$$

where S_r is shear strength (kPa), c' is effective cohesion (kPa), σ is normal stress (kPa), μ_a is pore air pressure (kPa), μ_w is pore-water pressure (kPa), $(\mu_a - \mu_w)$ is matric suction, or negative pore-water pressure (kPa), and $\tan \phi^b$ is the rate of increase in shear strength with increasing matric suction.

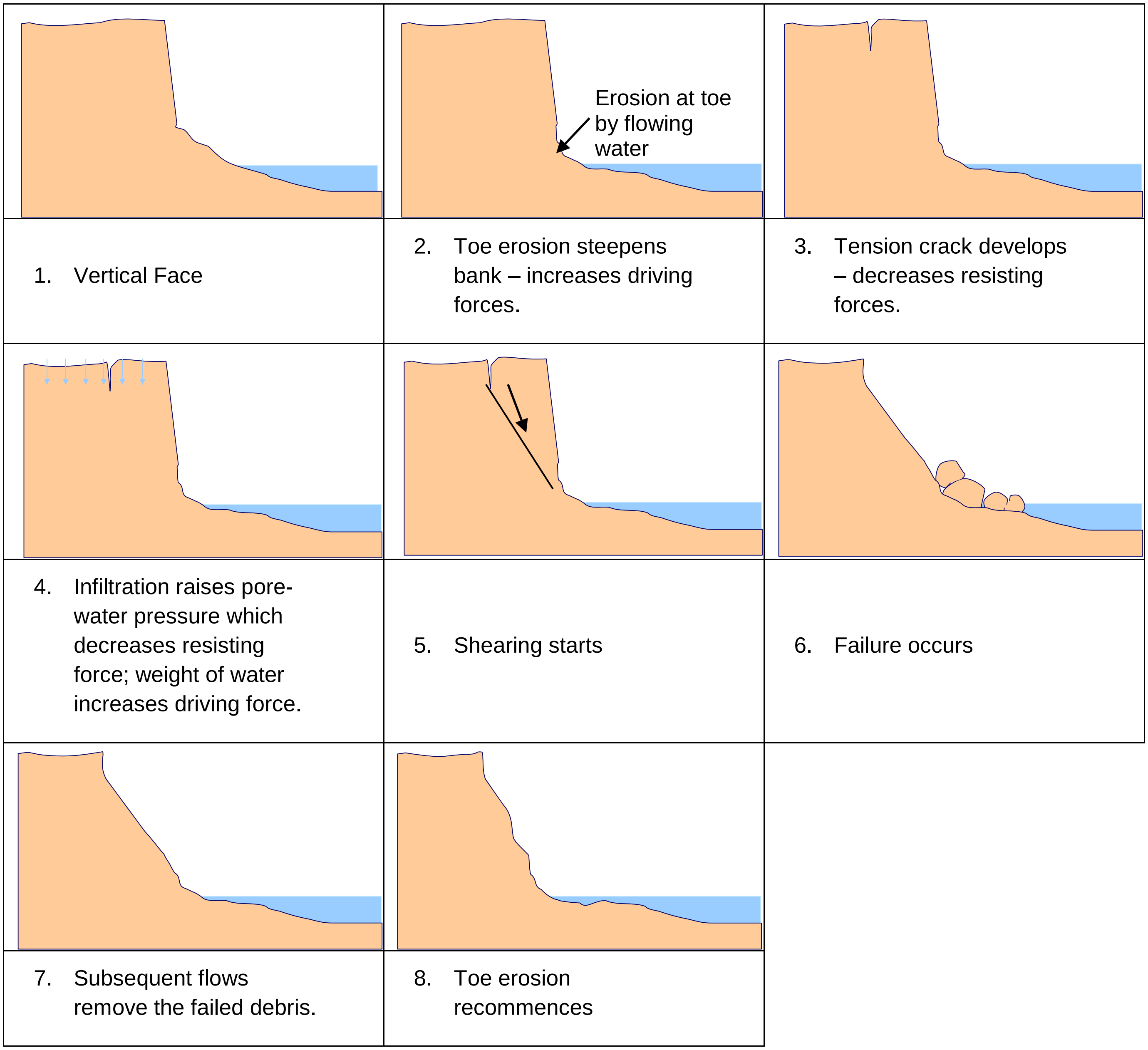

Figure 2-1 Conceptual model of bank and bar edge retreat that stresses the importance of the interaction of hydraulic forces that cause steepening of the lower part of the face, resulting in failure of the bank mass.

2.2 The Dynamic Bank Stability and Toe Erosion Model (BSTEM-Dynamic)

The Bank Stability and Toe-Erosion Model (BSTEM; Simon *et al.*, 1999) combines three limit-equilibrium methods that calculate the Factor of Safety (F_s) of multi-layer streambanks. The methods employed within BSTEM are horizontal layers (Simon *et al.*, 1999), vertical slices with tension crack (Morgenstern and Price, 1965) and cantilever failures (Thorne and Tovey, 1981). All three methods account for the strength of up to five soil layers, the effect of pore-water pressure (both positive and negative (matric suction)), confining pressure due to streamflow and soil reinforcement due to vegetation. This description will focus upon the first and third methods as the second method has not been used herein due to the absence of observed tension cracks in the field. All model runs are for one bank only, with each site being independent of each other. Additionally, the model does not contain sediment transport or routing functions.

2.2.1 Assessing Geotechnical Failure

The enhanced bank-stability sub-model in the current version of BSTEM-Dynamic (Simon et al., 2011) incorporates a random walk search algorithm for the minimum Factor of Safety, F_s. F_s is the ratio between the resisting and driving forces acting on a potential failure block. A value of unity indicates that the driving forces are equal to the resisting forces and that failure is imminent (F_s = 1.0). Instability exists under any condition where the driving forces exceed the resisting forces (F_s < 1.0), conditional stability is indicated by F_s values between 1.0 and 1.3, with stable bank conditions having a F_s value of >1.3. The Factor of Safety (F_s) of the horizontal layer method is given by:

$$F_s = \frac{\sum_{i=1}^{I}\left(\left[c_i' + c_r\right]L_i + \left(\mu_a - \mu_w\right)_i L_i \tan\phi_i^b + \left[W_i \cos\beta - \mu_{ai}L_i + P_i\cos(\alpha-\beta)\right]\tan\phi_i'\right)}{\sum_{i=1}^{I}\left(W_i \sin\beta - P_i \sin[\alpha-\beta]\right)} \quad (5)$$

where c_i' = effective cohesion of i^{th} layer (kPa), L_i = length of the failure plane incorporated within the i^{th} layer (m), W_i = weight of the i^{th} layer (kN), P_i = hydrostatic-confining force due to external water level (kN m^{-1}) acting on the i^{th} layer, β = failure-plane angle (degrees from horizontal), α = local bank angle (degrees from horizontal), and I = number of layers.

The cantilever shear failure algorithm results from inserting β = 90° into equation 5. F_s is given by:

$$F_s = \frac{\sum_{i=1}^{I}\left(c_i' L_i + \left(\mu_a - \mu_w\right)_i L_i \tan\phi_i^b + \left[P_i \sin\alpha - \mu_{ai}L_i\right]\tan\phi_i'\right)}{\sum_{i=1}^{I}\left(W_i + P_i\cos\alpha\right)} \quad (6)$$

The F_s is the ratio of the shear strength of the soil to the weight of the cantilever. The inclusion of α-terms in equation 6 ensures that if the bank is partially or totally submerged, the weights of the layers affected by water are correctly reduced irrespective of the geometry of the basal surface of the overhang.

2.2.2 Modeling Movement of the Groundwater Table

It is apparent from equations 3, 4, 5 and 6 that the elevation of the groundwater table is an important parameter controlling soil shear strength. A simplified one-dimensional (1-D) groundwater model, based on the 1-D Richards Equation, is used to simulate the motion of the groundwater table. This model assumes that the dominant pressure gradient within a streambank is the difference between the groundwater table elevation and the in-channel water surface elevation (i.e. it neglects the influence of infiltrating precipitation). Assuming that water infiltrates either into or out of the bank along a horizontal plane of unit length and computing distance-weighted mean soil properties between these two elevations, the simplified equation can be written as:

$$\frac{\partial h}{\partial t} - K_r K_{sat} = 0 \tag{7}$$

where h = groundwater elevation (m), t = time (s), and $K_r K_{sat}$ = relative permeability × saturated hydraulic conductivity. K_r is evaluated as $K_r = \Theta^{1/2}\left[1-\left(1-\Theta^{1/b}\right)^b\right]^2$, where Θ = soil saturation and, following van Genuchten (1980), Θ is evaluated as:

$$\Theta = \Theta_r + \frac{\Theta_s - \Theta_r}{\left[1+\left(\frac{[z-h]}{l}\right)^{1/1-m}\right]^m} \tag{8}$$

where the subscripts r and s denote the residual moisture content and saturated moisture content, l and m are curve-fitting parameters and z is the water surface elevation (m). If $h \geq z$, $K_r = 1$.

2.2.3 Assessing Hydraulic Erosion

The magnitude of bank-face and bank-toe erosion and the extent of bank steepening by hydraulic forces are calculated using an algorithm that computes the hydraulic forces acting on near-bank zone during a particular flow event. The boundary shear stress exerted by the flow on each node is estimated by dividing the flow area at a cross-section into segments (Figure 2-2) that are affected only by the roughness of the bank or the bed and then further subdividing to determine the flow area affected by the roughness on each node (e.g. Einstein, 1942). The hydraulic radius of a segment, R_i, is the area of the segment, A_i, divided by the wetted perimeter of the segment. The boundary shear stress active at the node i may then be estimated as:

$$\tau_{oi} = \rho g R_i S \tag{9}$$

where S = channel gradient (m m^{-1}).

Flow resistance in an open channel is a result of viscous and pressure drag over its wetted perimeter. For a vegetated channel, this drag may be conceptually divided into three components: (1) the sum of viscous drag on the ground surface and pressure drag on particles or aggregates small enough to be individually moved by the flow (grain roughness); (2) pressure drag associated with large non-vegetal boundary roughness (form roughness); and (3) drag on vegetal elements (vegetal roughness) (Temple *et al*., 1987). As energy lost to the flow represents work done by a force acting on the moving water, the total boundary shear stress may also be divided into three components:

$$\tau_o = \tau_{og} + \tau_{of} + \tau_{ov} \tag{10}$$

where the subscripts g, f and v signify the grain, form and vegetal components of the boundary shear stress, respectively.

If it is assumed that these components may be expressed in terms of a Manning's coefficient for each, and Manning's equation is assumed to apply for each component, equation 9 can be rewritten as (Temple, 1980):

$$n^2 = n_g^2 + n_f^2 + n_v^2 \tag{11}$$

where n = Manning's roughness coefficient (s $m^{-1/3}$). Grain roughness is estimated for each node on the bank profile using the equation of Strickler (Chow, 1959):

$$n_g = 0.0417\ (D_{50}^{1/6}) \qquad (12)$$

Combining equations 10 and 11, the effective boundary shear stress, the component of the boundary shear stress acting on the boundary in the absence of form and vegetal roughness, may be computed as:

$$\tau_g = \tau_o\ (n_g^2 / n^2) \qquad (13)$$

The rate of erosion of bank-face and bank-toe materials can then be calculated using an excess shear approach (Partheniades, 1965).

An average erosion rate (in m/s) is computed for each node and time-step where the boundary shear stress exceeds the critical shear stress of the bank or toe material. This erosion rate is then integrated with respect to time to yield an average erosion distance. This method is similar to that employed in the CONCEPTS model (Langendoen, 2000):

$$E = k\ \Delta t\ (\tau_o - \tau_c) \qquad (14)$$

where E = erosion distance (cm), k = erodibility coefficient (cm^3/N-s), Δt = time step (s), and τ_c = critical shear stress (Pa).

Resistance of bank-toe and bank-surface materials to erosion by hydraulic shear is handled differently for cohesive and non-cohesive materials. For cohesive materials the relation developed by Simon *et al*. (2010; 2011) using a submerged jet-test device (Hanson, 1990) is used:

$$k = 1.6\ \tau_c^{-0.826} \qquad (15)$$

For non-cohesive materials the following relation is used:

$$k = 0.1\ \tau_c^{-0.5} \qquad (16)$$

This relationship was analytically compared with excess shear stress-based bedload transport functions proposed by Du Boys (1879), Schoklitsch (1914), O'Brien and Rindlaub (1934), Shields (1936), Bagnold (1956), van Rijn (1984) and Wu *et al*. (2000) and was found to provide reasonable estimates of k for particles in the medium to coarse sand range.

During the dynamic simulations described herein, the erosion distance during a time-step is computed by integrating the erosion rate within the time-step by the time-step size. It must be stressed that the model is incapable of routing flow and sediment, so that estimates of erosion are only valid for "clear-water" conditions where the amount of hydraulically-controlled sediment being transported by the flow is lower than sediment transport capacity.

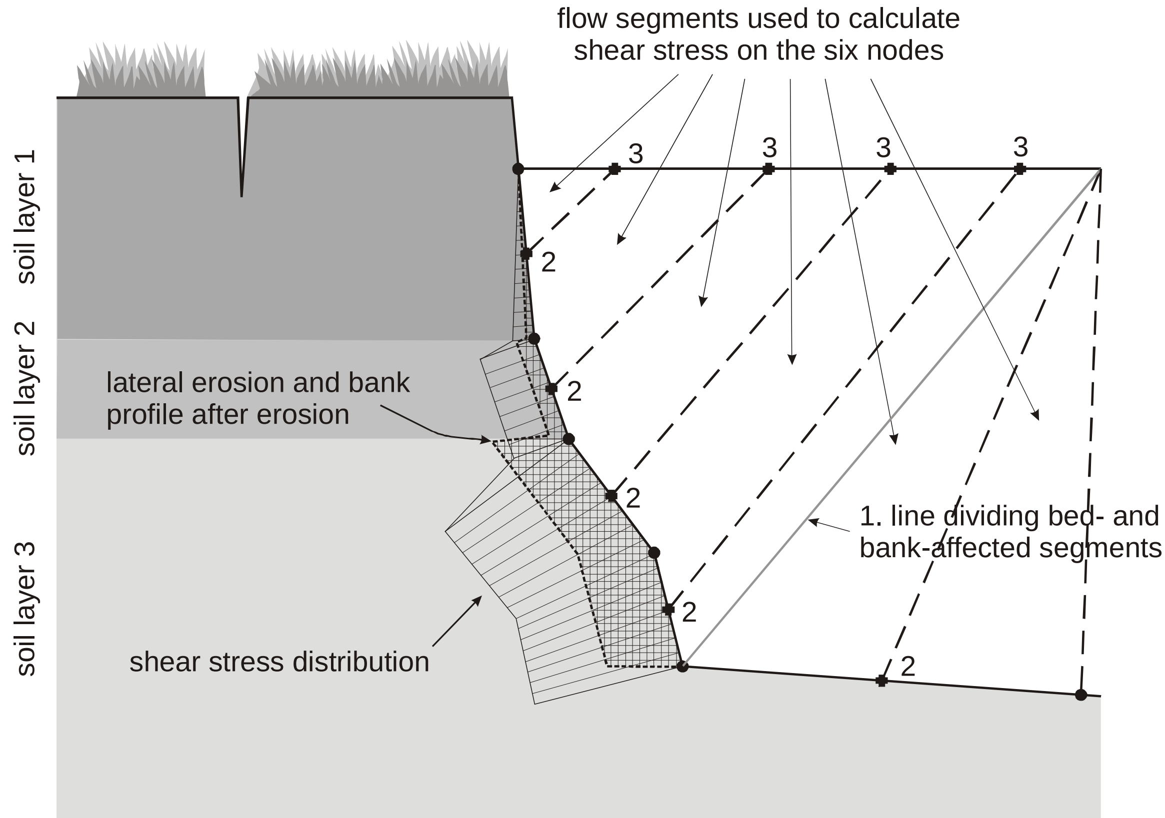

Figure 2-2 Segmentation of local flow areas and hydraulic radii.

2.2.4 Root Reinforcement by Riparian Vegetation

Soil is generally strong in compression, but weak in tension. The fibrous roots of trees and herbaceous species are strong in tension but weak in compression. Root-permeated soil, therefore, makes up a composite material that has enhanced strength (Thorne, 1990). Numerous authors have quantified this reinforcement using a mixture of field and laboratory experiments. Endo and Tsuruta (1969) used in situ shear boxes to measure the strength difference between soil and soil with roots. Gray and Leiser (1982) and Wu (1984) used laboratory-grown plants and quantified root strength in large shear boxes.

Many studies have found an inverse power relationship between ultimate tensile strength, *Tr*, and root diameter, *d* (examples include but are not limited to: Waldron and Dakessian, 1981; Riestenberg and Sovonick-Dunford, 1983; Coppin and Richards, 1990; Gray and Sotir, 1996; Abernethy and Rutherfurd, 2001; Simon and Collison, 2002; Pollen and Simon, 2005; Fan and Su, 2008):

$$T_r = e(1000d)^f \qquad (17)$$

where *e* = multiplier (MPa m^{-f}), and *f* = exponent (dimensionless) in the root tensile strength- diameter function, respectively. Note that *f* is always negative. Root strength (in kN) can therefore be evaluated as the product of the root area, A_r ($\pi d^2/4$), and the ultimate tensile strength, T_r:

$$T_r A_r = \frac{e\pi\left(1000^{1+f}\right)d^{2+f}}{4} \qquad (18)$$

Smaller roots are stronger per unit area (higher ultimate tensile strength), but the larger cross-sectional area of larger diameter roots means that the peak load they can withstand before breaking, is higher than that of small roots.

Wu et al. (1979, after Waldron, 1977) developed a widely-used equation that estimates the increase in soil strength (c_r) as a function of root areal density and root distortion during shear:

$$c_r = \frac{1}{A}\sum_{i=1}^{i=I}\left(A_r T_r\right)_i \left[sin(90-\zeta) + cos(90-\zeta) tan\,\phi'\right] \qquad (19)$$

where c_r = cohesion due to roots (kPa), T_r = tensile strength of roots (kPa), A_r = area of roots in the plane of the shear surface (m^2), A = area of the shear surface (m^2), I = total number of roots crossing the shear plane, the subscript i = i^{th} root, and

$$\zeta = \tan^{-1}\left(\frac{1}{\tan\theta + \cot\chi}\right) \qquad (20)$$

where θ = angle of shear distortion (degrees), and χ = initial orientation angle of fiber relative to the failure plane (degrees).

Pollen et al. (2004) and Pollen and Simon (2005) found that models based on equation 19 tend to overestimate root reinforcement because it is assumed that the full strength of each root is mobilized during soil shearing and that the roots all break simultaneously. This overestimation was largely corrected by Pollen and Simon (2005) by developing a fiber-bundle model (RipRoot) to account for progressive breaking during mass failure. RipRoot was validated by comparing results of root-permeated and non-root-permeated direct-shear tests. These tests revealed that, relative to results obtained with the perpendicular model of Wu *et al.* (1979), accuracy was improved by an order of magnitude, but some error still existed (Pollen and Simon, 2005).

One explanation for the remaining error in root-reinforcement estimates lies in the fact that observations of incised streambanks suggest that, when a root-reinforced soil shears, two mechanisms of root failure occur: root breaking and root pullout. The anchorage of individual leek roots was studied by Ennos (1990), who developed a function for pullout forces based on the strength of the bonds between the roots and soil:

$$F_P = \pi d \tau_s L_r \qquad (21)$$

where F_P = pullout force for an individual root (N), and L_r = root length (m), which can be estimated in the absence of field data using $L_r = 123.1\, d^{0.7}$ (Pollen, 2007).

The pullout force was not accounted for in the original version of RipRoot (Pollen and Simon, 2005) and so the role played by spatial-temporal variations in soil shear strength was neglected. Pollen (2007) tested the appropriateness of equation 21 by making field measurements of the forces required to pull out roots. Pullout forces were then compared with breaking forces obtained from testing and the RipRoot model was modified to account for both breaking and pullout.

3 Field Data Collection

This study was structured in two phases: *in-situ* field data collection discussed in this chapter, and model runs using BSTEM-Dynamic Ver. 1.0, discussed in Chapter 4. Field data was collected at multiple locations across PRRIP cross-sections 2, 13 and 20 within the Elm Creek Reach (Figure 3-1) to characterize the hydraulic and geotechnical characteristics of the materials and vegetation that could influence lateral erosion, and thus associated sediment dynamics and channel planform.

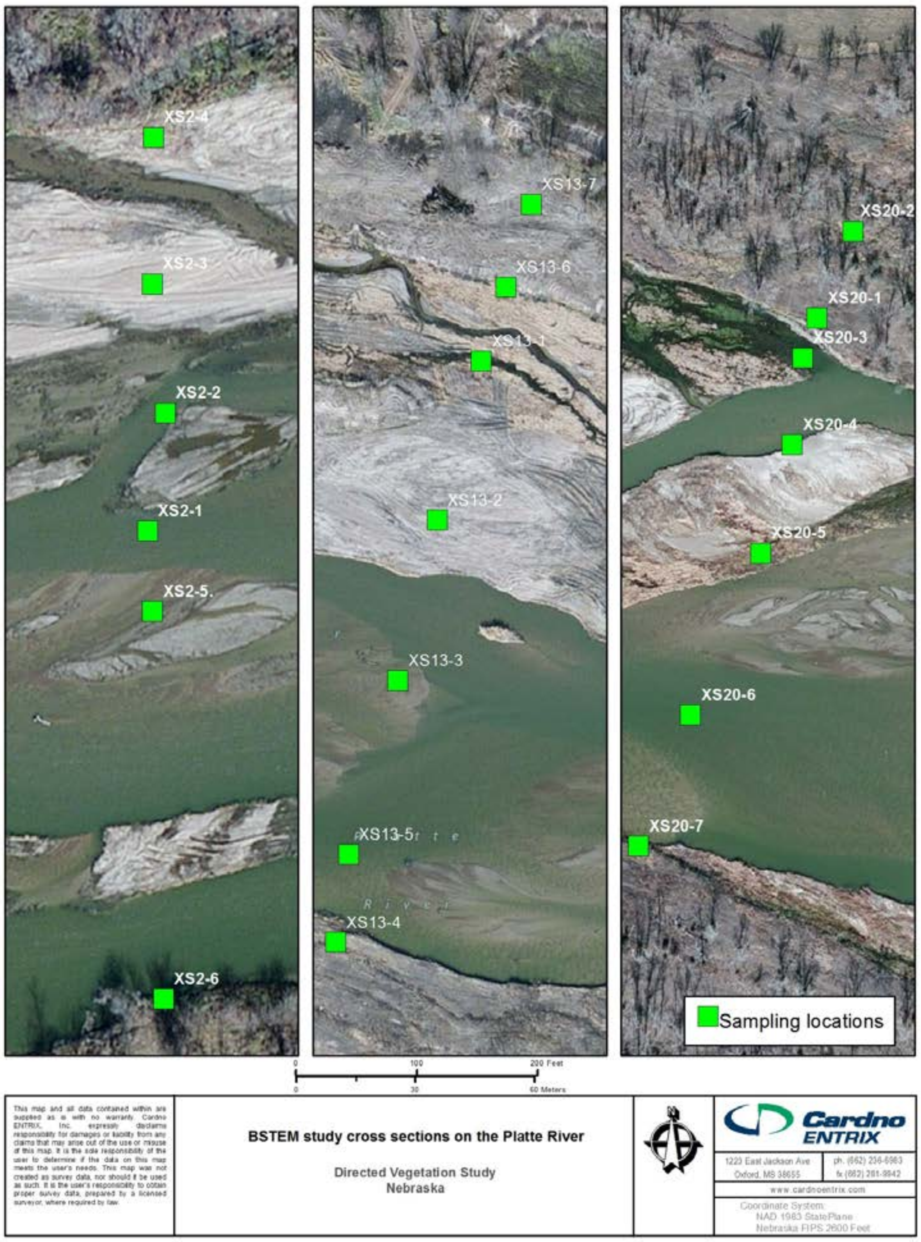

Figure 3-1 Sampling locations within each cross section. Water levels during field investigations were lower than those seen in the aerial photograph taken from Google Earth. In addition, with the very dynamic nature of the bars in this reach, "bar edges" identified during fieldwork may be shown as "bar" locations in these photos.

Hydraulic and geotechnical resistance tests were attempted using the *Submerged Mini-Jet Test Device* and Iowa Borehole Shear Tester respectively. The sandy materials, however, were not conducive to these methods. . *In lieu* of this, the Humboldt Torvane and pocket Penetrometer were used to determine total shear strength and determine unconfined material compressive strength. These data were then used as input parameters for BSTEM-Dynamic Ver. 1.0 which was calibrated using May and August 2011 cross-section surveys and flow data from the USGS gage 06768000 Platte River near Overton, NE for the same time period. Once the model had been calibrated, further model runs were carried out to examine the effect of different vegetation scenarios on lateral erosion of the bank and bar locations modeled. BSTEM model output provided volumes of erosion and timing of erosion events for each modeled scenario.

3.1 *In Situ* Field Data Collection and Material Properties

3.1.1 Quantifying Geotechnical Resistance to Failure

As bank stability is a function of the strength of the bank material to resist collapse under gravity, measurements of the components of shearing resistance (or shear strength) were required to model bank stability at three sites within the four mile PRRIP study reach. Attempts were made to use the Iowa Borehole Shear Tester (BST) to determine parameters such as apparent cohesion and material friction angle. However, due to the non-cohesive nature of the soils, bore holes collapsed and reliable tests could not be completed using this instrumentation. In place of the BST, the Humboldt Torvane and pocket Penetrometer were used to determine material shear strength (Figure 3-2). The Torvane Shear Device is used to obtain rapid measurements of total shear strength from a smooth surface of any inclination. The vane is pressed firmly into the materials to the depth of the vanes and rotated under constant normal force until the material fails. The maximum resistance is then read directly from the dial. The test takes a matter of seconds to complete, allowing for multiple tests to be conducted in a short time. Five tests were conducted to define each material. While the Torvane Shear does provide a good indication of shear values and has a very good correlation between its readings and those of an unconfined compression test, readings are dependent on several factors, including operator methods and rate of load, progressive failure, plane orientation, and varying moisture levels. (Humboldt Manufacturing, 2011). Differences in operator methods were minimized by having just one member of staff conduct all measurements. The Torvane shear, however, provides values of total shear strength that combine the cohesive and frictional components. Because the tested materials have virtually no cohesion, Torvane results represent frictional strength alone. Values of matric suction were obtained with an in-field digital tensiometer.

The last parameter value needed to calculate effective cohesion (c') required as input to BSTEM, was normal stress (σ). This was obtained using a two-step process. A Pocket Penetrometer (Figure 3-2), generally used to measure compressive strength, provided a measure of the normal stress required to push a piston of 0.05 in^2 (0.32 cm^2) ¼" (6.35 mm) into the material. The stress required to accomplish this is then read directly from the scale indicator. Assuming that the stress required to push the Torvane Device is directly proportional to the stress required to insert the Penetrometer, a relation was developed between the area of the vanes multiplied by the depth (for the Torvane) and the area of the piston multiplied by the depth (for the Penetrometer). This value was then multiplied by the value obtained with the Penetrometer to obtain the normal stress (σ) employed during the Torvane tests. Values of effective cohesion (*c'*) were obtained by then re-arranging the Mohr-Coulomb shear strength criterion for unsaturated soils (Fredlund *et al.,* 1978) and solving for *c'*.

$$\tau_s = \left[c' + (\mu_a - \mu_w)\tan\phi^b + (\sigma - \mu_a)\tan\phi'\right] \qquad (22)$$

where τ_s = soil shear strength (kPa), c' = effective cohesion (kPa), μ_a = pore-air pressure (kPa), μ_w = pore-water pressure, $(\mu_a - \mu_w)$ = matric suction (kPa), ϕ^b is the angle describing the increase in shear strength due to an increase in matric suction (degrees) and ϕ' = effective angle of internal friction (degrees).

Figure 3-2 Left: Humboldt Torvane used to define material shearing resistance. Right: Pocket Penetrometer used to determine unconfined material compressive shear strength.

3.1.1.2 Measured shear strength values

The materials at the bar and bank edges of the three cross sections studied were sands and fine gravels with little to no cohesion (Table 3-1). Frictional strength values calculated from the Torvane data ranged from 0.00 to 0.806 kPa where little or no vegetation was present, In materials with low cohesion values such as these, the presence of even a few roots can dramatically increase the cohesion of the material. This is shown in the Torvane data where up to 7.60 kPa was measured in a location where vegetation of a moderate density was present on the bar. Rows highlighted in green in Table 3-1 indicate locations where field data were used as input to BSTEM. The histogram in Figure 3-3 emphasizes the finding that the vast majority of locations tested (72.7 %) had low cohesion values of less than 1 kPa.

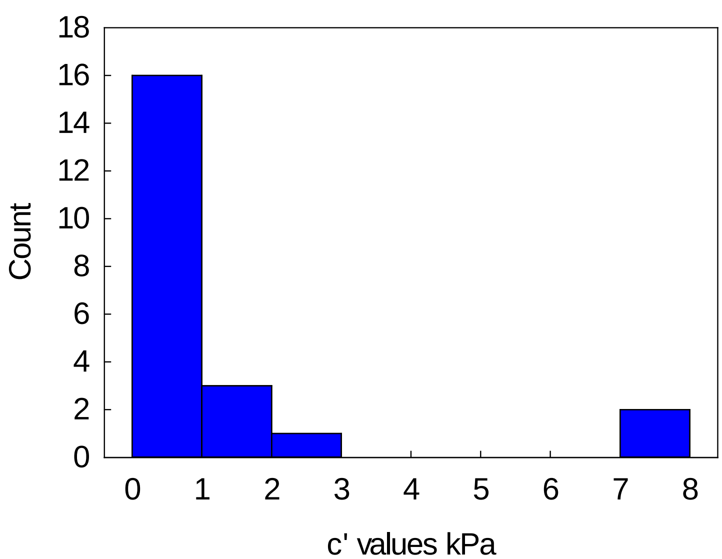

Figure 3-3 Histogram of cohesion values calculated from Torvane data collected *in situ.*

Table 3-1 Field data collected in situ to measure shear strength of the bar and bank edges. Rows highlighted in green indicate locations where field data were used as input to BSTEM. Cross sections 2, 13 and 20 were chosen to cover the upper, middle and end of the Elm Creek Complex Reach.

Site	Bank/Bar description	Average Frictional Strength calculated from *in situ* Tore Vane data in kPa
XS2-1	Ltoe	0.714
XS2-2	Lbank/Bar	0.00
XS2-3	Lbank/Bar	0.555
XS2-4	Lbank/Bar	0.257
XS2-5	Lbar in channel	0.527
XS2-6	RB	0.613
XS13-1	Lbar Left	0.355
XS13-2	Lbar Right	0.00
XS13-3	Mbar mid	0.518
XS13-4	Rbank	2.21
XS13-5	Rbar - mid	1.04
XS13-6	Lbank	0.901
XS13-7	Lbtop	7.60
XS20-1	Lbank	0.809
XS20-2	Lbank/Bar	0.797
XS20-3	Lbar - mid	0.959
XS20-4	Mbar - right	7.94
XS20-5	Mbar - Left	1.76
XS20-6	Rbar - Right	0.558
XS20-7	RB	0.00
XS20-7	RB	1.30
XS20-7	RB	0.806

3.1.2 Quantifying Hydraulic Resistance to Failure

All of the materials encountered on the bank toes and bank surfaces had very low cohesion. Because of this, the submerged mini-jet test device was not an appropriate tool for determining properties of hydraulic resistance. Values of critical shear stress of the surface sediments, therefore, were based on the particle-size distribution of the non-cohesive materials. The Shields (1936) criterion is used for resistance of non-cohesive materials as a function of roughness and particle size (weight), and is expressed in terms of a dimensionless critical shear stress (Figure 3-2):

$$\tau^*_c = \tau_o / [(\rho_s - \rho_w)\, g\, D]$$

where τ^*_c = critical dimensionless shear stress, ρ_s = sediment density (kg/m^3), ρ_w = water density (kg/m^3), g = gravitational acceleration (m/s^2), and D = characteristic particle diameter (m).

If materials were composed primarily of sand and fine gravel, a bulk sample was obtained and returned to a laboratory for an analysis of particle size. For coarser materials, the intermediate axis of 100 particles were measured and recorded. If more than 15 particles were characterized as sand or finer during the particle count, a bulk sample of these finer materials were obtained to be combined with the results of the particle count. Results of the material analyses were then applied to the equation above to obtain τ_c.

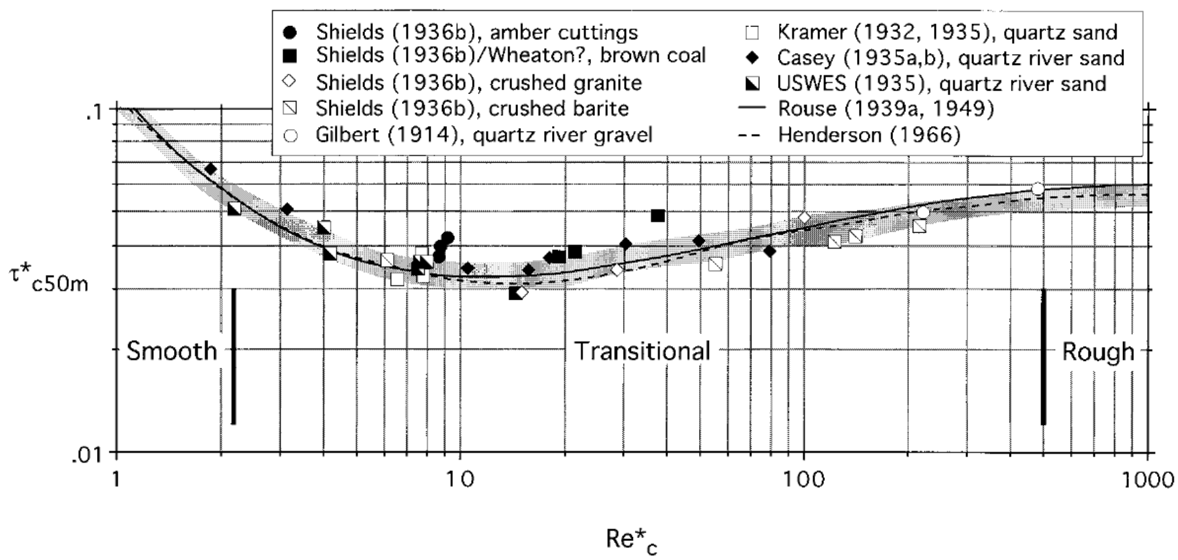

Figure 3-4 Shields diagram for incipient motion (modified from Buffington, 1999). The y-axis is defined by $\tau_o = \gamma RS$ where τ_o is the mean bed shear stress, in N/m^2 (Pa) and R is the hydraulic radius, in meters and the x-axis is defined by $\tau_o = \tau_{og} + \tau_{of} + \tau_{ov}$ where the subscripts *g*, *f* and *v* signify the grain, form and vegetal components of the boundary shear stress, respectively

3.1.2.2 Measured Critical Shear Stress Values

The material at the bank and bar edges of each studied cross section was dominated by particle sizes in the sand and fine gravel ranges. These were characterized through bulk samples that were sent for laboratory analysis to determine particle size breakdowns and d_{50} values for BSTEM data input. Values of d_{50} ranged from 0.26 to 4.00 mm; the median value of 0.615 showed that the overall data set was skewed towards the lower end of that particle size range, indicating a predominance of sand particles rather than fine gravels (Figure 3-5). To use the particle size data collected in BSTEM, the d_{50} values were converted to corresponding critical shear stress values. The rows highlighted in green in Table 3-2 indicate the samples that were used as input data, based on their proximity to the bank and bar locations modeled in BSTEM.

Table 3-2 Particle size d_{50} from samples taken at the three cross sections studied, and corresponding *Tc* values to be used in BSTEM Dynamic 1.0, calculated using the Shields entrainment curve (1936). Rows highlighted in green indicate locations where field data were used as input to BSTEM.

Sample Location	d_{50} in mm	Corresponding critical shear stress (Pa)
XS2-1 Toe Left	0.35	0.25
XS2-3 Left bank face bar	1.20	0.86
XS2-5 Left Bar	1.60	1.14
XS2-6 Right bank face	0.28	0.20
XS13-1 Left bar - left	0.50	0.36
XS13-2 Left bar - right	1.40	1.00
XS13-3 Mid bar - mid	0.80	0.57
XS13-4 Right bank	0.65	0.46
XS13-5 Right bank mid	0.65	0.46
XS13-6 Left bank face	0.27	0.19
XS13-7 Left bank bar	0.58	0.41
XS20-1 Left bank	0.40	0.29
XS20-2 Left bank bar	0.65	0.46
XS20-3 Left bar mid	0.36	0.26
XS20-4 Mid bar left	0.50	0.36
XS20-5 Mid bar right	4.00	3.89
XS20-6 Right bar	0.33	0.24
XS20-7 Right bank face layer 1	0.26	0.19
XS20-7 Right bank face layer 2	0.72	0.51
XS20-7 Right toe	0.76	0.54

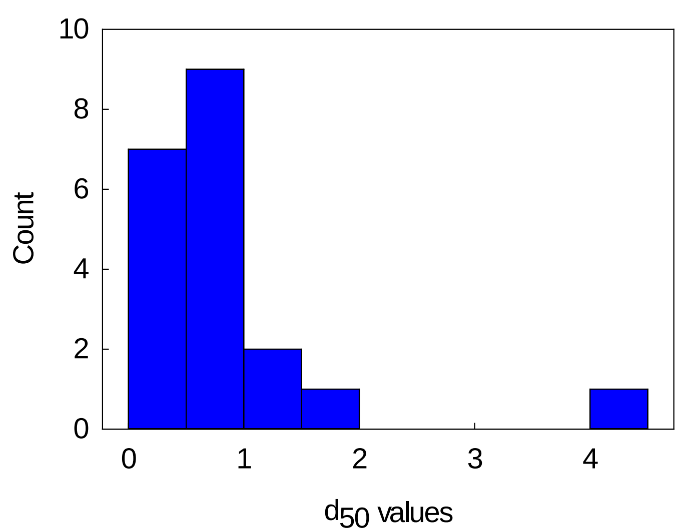

Figure 3-5 Histogram showing the distribution of d_{50} values in the bank and bar samples taken at XS2, XS13, and XS20.

3.1.3 Reinforcement due to Vegetation Roots

As well as hydraulic and geotechnical material properties, it was also important to establish the added resistance to hydraulic and geotechnical erosion provided by vegetation present on the bar or bank-top and -face. Vegetation composition was determined and stem counts performed in the field. In addition, root systems of the riparian species were examined and documented using the wall-profile method (Bohm, 1979), where exposed roots of the study species could be seen along bank and bar edges. Root diameters were measured and recorded according to depth in the bank-face profile to determine root density per square meter of bank or bar face, and the distribution of roots within different size classes. These stem and root density measurements were used to quantify the effects of each species (cottonwoods <2 years of age, Reed canarygrass and *Phragmites*) on the shear strength (geotechnical) and critical shear stress (hydraulic) parameters for the BSTEM runs with vegetation.

3.1.3.1 Measured Root and Stem Properties

All of the stem density measurements taken fell within the ranges measured in the previous directed vegetation study (Pollen-Bankhead et al., 2010). Measured rooting densities ranged from 10 to 30 roots per m^2 of bank or bar face for 1 year old cottonwood seedlings, and from 400 to ~1500 roots per m^2 for Reed canarygrass (Table 3-3). Application of the stem and root density data to BSTEM will be discussed in detail in Section 4.3.

Table 3-3 Maximum root densities measured in the Central Platte for the species of interest in this study.

Species	Minimum number of roots measured per m^2 of bank/bar face	Maximum number of roots measured per m^2 of bank/bar face	Number of sample quadrats
Cottonwood (< 1 year)	10	30	5
Cottonwood (1-2 years old)	10	54	7
Reed canarygrass	400	1480	3
Phragmites	100	275	5

4 BSTEM Dynamic Runs

4.1 Flow Data and Modeling Locations

Mean daily discharge data from the USGS gauging station 06768000 Platte River near Overton, NE May 1st to August 31st 2011 (Figure 4-1) were used as the flow input parameter in BSTEM Dynamic. The use of this flow period in BSTEM was selected for two reasons. First, this was a time period bounded by repeated cross sections surveys to be used for model calibration. Second, the flow record contained a range flows, so the effects of both low flows and a SDHF event of >8,000 ft^3s^{-1}, on bar and bank erosion could be examined from the BSTEM Dynamic output.

The discharge data were input to a standard normal depth spreadsheet, populated with the May 2011 cross section for each of the three cross sections visited (XS2, 13 and 20). The normal depth sheet was run with a channel slope value of 0.001 (Pollen-Bankhead et al., 2010) to determine flow stage for each daily time step within BSTEM, under a range of Manning's n values.

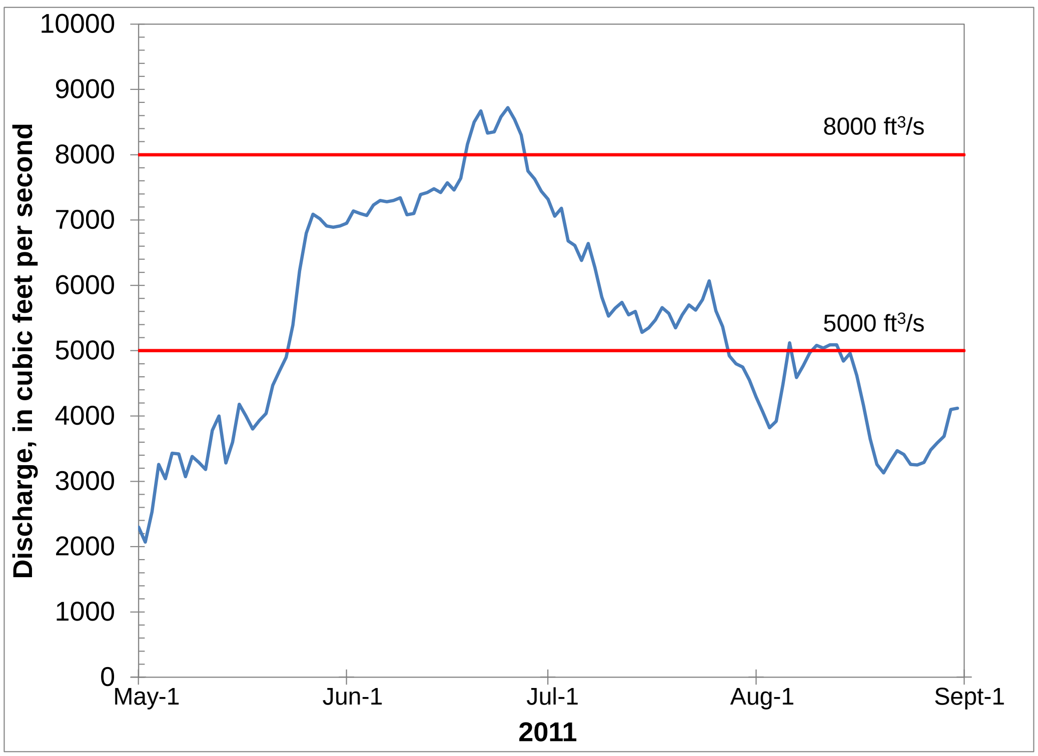

Figure 4-1 Flow data at the USGS gage 06768000 Platte River near Overton, NE for the calibration and modeling period May 1st to August 31st 2011, used as input for BSTEM-Dynamic.

For each of the three cross sections, one bank edge and one bar edge were selected for calibration and further analysis with various vegetation scenarios in BSTEM Dynamic 1.0 (Table 4-1).Bank edges tended to be fairly stable over the May 2011 to August 2011 calibration period; in each case the right bank was selected for further investigation in BSTEM runs. As a contrast to the relatively stable banks, the bar edges selected, were chosen for their dynamic nature, with measureable change over the calibration period.

Table 4-1 Locations within each cross section selected for further BSTEM analysis.

XS2	XS2-3 Bar Edge
	XS2-6 Right Bank Edge
XS13	XS13-2 Bar Edge
	XS13-6 Right Bank Edge
XS20	XS20-6 Bar Edge
	XS20-7 Right Bank Edge

4.2 Calibration of BSTEM Dynamic 1.0 using May 2011 and August 2011 cross sections

Bank and bar edges from the May and August 2011 repeat surveys were extracted for the three bar edges and three bank edges to be modeled. Measured eroded volumes between the two surveys were calculated using Sigmaplot (Table 4-2), and were then used to compare with eroded volumes simulated with BSTEM during the calibration process. The bank edges were all relatively stable over the calibration period, with only small volumes of erosion and deposition evident from the repeat cross sections. In contrast, the bar edges selected for modeling had noticeable changes over the calibration period, with the XS20-6 bar edge, for example, moving over 20 m during just 3 months.

To calibrate BSTEM Dynamic, the May to August 2011 time period was run, using different Manning's n values. The effect of this was to vary the shear stresses being applied to the banks and bars in BSTEM, and thus the predicted erosion volumes over the calibration period. Measured eroded volumes versus those obtained in the best calibration run for each modeled location are shown in Table 4-2, along with the associated Manning's n value. Calibration of BSTEM in this way was necessary because BSTEM is not a sediment transport model; the 1D toe erosion algorithm assumes clear water scour, and does not have any way of calculating how much sediment is already entrained in the water, and the excess energy available for further entrainment. Calibrating around Manning's n, allows for adjustment of the applied shear stresses to correct for this. Channel roughness and corresponding Manning's n values vary along a channel, but would be expected to be towards the lower end of the normal range of n values (0.02 to 0.07; Table 4-2) in this relatively smooth channel. Indeed, calibration runs resulted in Manning's n values of 0.035 and less for four of the six sites to be modeled. Manning's n values required for calibration at the two sites at XS 20 were higher (0.06; Table 4-2) suggesting that the assumption of clear water scour was more of an issue at this cross section, than the other two sections modeled.

Table 4-2 Values of measured versus modeled eroded volumes from May 2011 to Aug 2011 at the study locations.

Site	Measured May to Aug 2011 Volume eroded (m^3/m of bar or bank edge)	Modeled May to Aug 2011 Volume eroded (m^3/m of bar or bank edge)	Manning's *n* from calibration run	% difference between measured and modeled
2-3 Bar	3.28	3.90	0.025	-18.9
2-6 Bank	0.270	0.550	0.024	-104
13-2 Bar	16.1	27.2	0.035	-68.9
13-6 L Bank	0.091	0.090	0.035	1.10
20-6 Bar	20.02	19.5	0.060	2.60
20-7 R Bank	1.21	1.38	0.060	-14.1

The measured versus modeled erosion volumes in Table 4-2 show relatively good agreement (within 20%) in four of the six cases. At locations XS2-6 and XS13-2, the greater difference between the measured eroded volume and modeled eroded volume was largely a result of the fact that the local bed level rose in the repeat surveys as a result of deposition. The process of deposition cannot be modeled in BSTEM so erosion volumes in the calibration runs were higher in these instances. As can be seen from the plots of May and August 2011 bank and bar edge profiles, with associated calibration runs (Figure 4-2), modeled lateral erosion distances, did however, closely match those measured in all cases, even in those cases where local bed elevation changed.

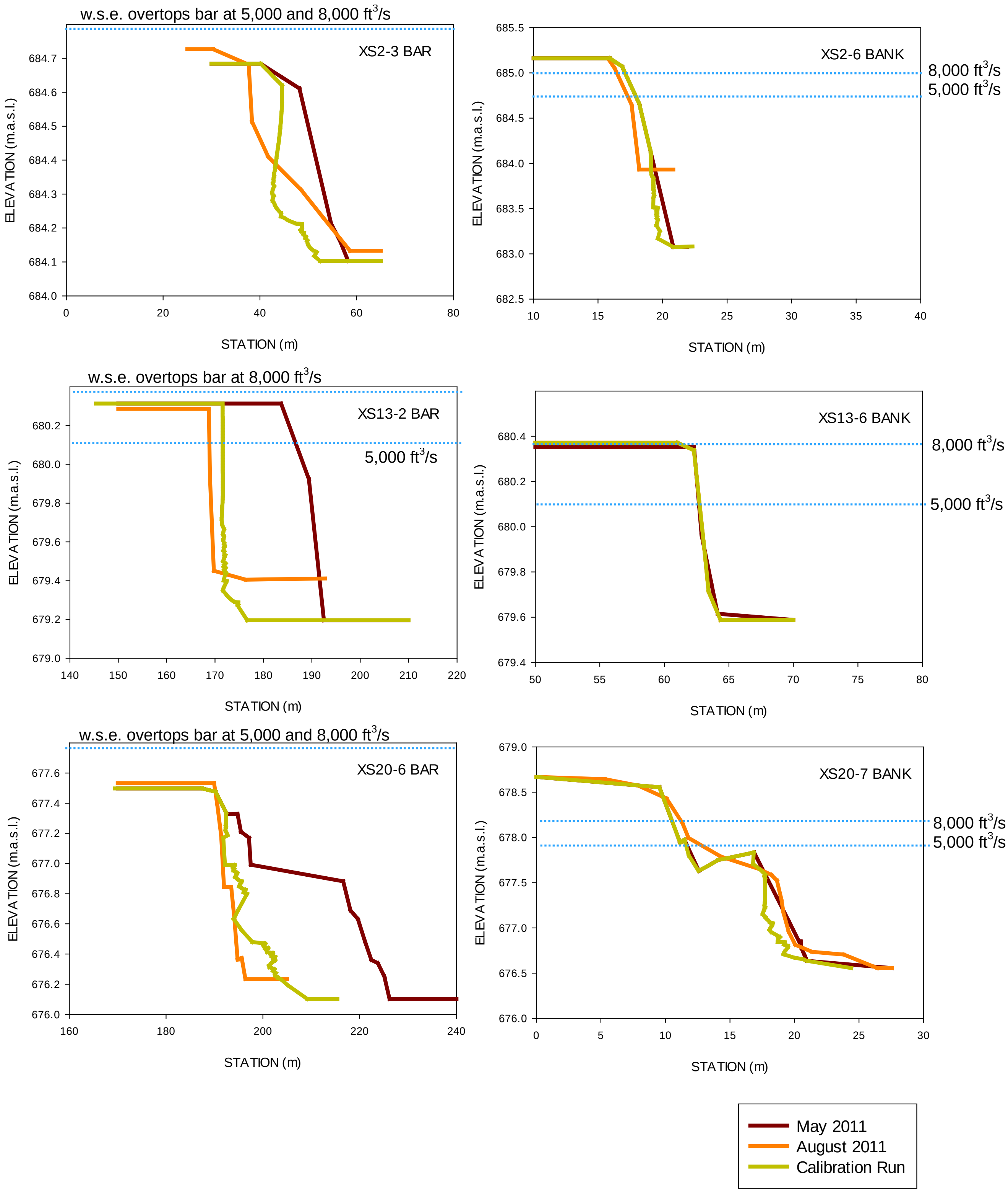

Figure 4-2 Calibration runs compared to measured May 2011 to August 2011 cross sections.

4.3 Vegetation Input parameters for BSTEM

To model the effects of vegetation on volumes and patterns of erosion at bar and bank edges, and to compare those values with the calibration runs, field data collected as part of this study and RipRoot runs performed in the first Directed Vegetation Study (Pollen-Bankhead et al., 2010), were used. These data informed us how the different species may affect both the geotechnical and hydraulic input parameters in the BSTEM model. The vegetation scenarios modeled in this current study were the same as those investigated in the first report by Pollen-Bankhead et al. (2010), allowing for comparison of results between the two studies. The vegetation scenarios modeled in BSTEM were cottonwood seedlings less than one year old (CW1), cottonwood seedlings 1-2 years old (CW2), Reed canarygrass (RCG) and *Phragmites* (PHRAG). Mechanical root-reinforcement increases the shear strength of the bank material (Pollen and Simon,2005; Pollen, 2007), while the presence of roots at the face of the bank or bar acts to increase the critical shear stress of the material (Simon et al., 2010). To account for roots in the BSTEM runs with vegetation, therefore, the cohesion of the bank/bar material was increased to account for root-reinforcement, and the critical shear stress of the material was increased to account for the effect of roots on the material's hydraulic parameters. The following sections describe the way in which these effects were quantified to account for vegetation within the BSTEM simulations.

4.3.1 Measured Root and Stem Properties to account for effects of roots on critical shear stress.

Root-density data collected in the field were used to inform the critical shear stress values input to BSTEM for the vegetation runs. A previous study by Simon et al. (2011) showed that the presence of roots in a streambank can increase the critical shear stress of the particles by up to a factor of ten. This increase in critical shear stress due to roots occurs as a result of two factors: binding of the particles by the roots, and protection of the particles by the roots themselves. In another study by the authors (Pollen-Bankhead and Simon, 2010), a non-linear relationship was found between decreasing volume of scour in a series of root-permeated jet tests, and increasing root volume within the soil. To determine the increase in tc that should be applied in each of the model runs with vegetation, the root densities shown in Table 4-3 were used in conjunction with the findings of these two studies as follows.

The maximum rooting density for Reed canarygrass was very similar to that in the jet tests in the Pollen-Bankhead and Simon (2010) study of switchgrass roots, that showed approximately a factor of ten reduction in eroded soil volume with this root density. As such, critical shear stress was increased by a factor of ten for this maximum rooting density in the Reed canarygrass runs. The increases in τ_c for the remaining vegetation runs were then estimated based on the assumption of a non-linear decrease in the effect of roots as rooting density declines (as per Pollen-Bankhead and Simon, 2010). Values for increases in τ_c for both minimum and maximum rooting densities measured in the field were thus estimated to use in BSTEM for each vegetation scenario (Table 4-4).

Table 4-3 Factor increase in τ_c values to account for variations in rooting densities for each set of vegetation runs in BSTEM Dynamic.

Species	Minimum Root Density Per m^2 Of Bank/Bar Face	Factor Increase In τ_c	Maximum Root Density per m^2 Of Bank/Bar Face	Factor Increase In τ_c
Cottonwood (< 1 year)	10	1.1	30	2
Cottonwood (1-2 years old)	10	1.1	54	2
Reed canarygrass	400	5	1500	10
Phragmites	100	2	250	5

4.3.2 Vegetation input parameters for runs with vegetation

Minimum and maximum values of root-reinforcement for the different species to be tested in BSTEM were obtained from the RipRoot Monte Carlo runs carried out in the first Directed Vegetation Report (Pollen-Bankhead et al., 2010) (Table 4-4). These runs used field data collected in the Central Platte to develop root tensile strength curves for each species, and stem and root densities also measured in the field.

At each bank and bar location to be modeled, two runs were performed for each species, to provide the minimum and maximum potential volumes of erosion. The first run in each case used the minimum root-reinforcement predicted for the study species in the Monte Carlo runs in Pollen-Bankhead et al. (2010), in conjunction with the minimum potential effect of roots on critical shear stress values. The second set of runs used the maximum predicted root-reinforcement values for each species from Pollen-Bankhead et al. (2010), combined with the maximum potential effect of roots on bank/bar edge critical shear stress values (Table 4-4). Calibrated Manning's *n* values from Table 4-2 were used in all runs with vegetation. For cottonwood seedlings and Reed canarygrass, modified cohesion and critical shear stress values were only applied to the top 0.5m of the bank or bar, to best replicate the typical rooting depths noted during fieldwork. In contrast, for *Phragmites*, modified cohesion and critical shear stress values were applied to the entire depth of the bar or bank, because this species was seen during root excavations to be capable of having rhizomes extending downwards greater than 1m.

Table 4-4 Modified input parameters for BSTEM to account for root-reinforcement due to vegetation and increased critical shear stress values due to the presence of roots.

<table>
<tr><th></th><th>CW1 min</th><th>CW1 max</th><th>CW2 min</th><th>CW2 max</th><th>RCG min</th><th>RCG max</th><th>PHRAG min</th><th>PHRAG max</th></tr>
<tr><td rowspan="2">Additional cohesion due to roots (kPa)</td><td>0.00</td><td>0.69</td><td>0.00</td><td>2.36</td><td>0.20</td><td>8.49</td><td>10.6</td><td>42.2</td></tr>
<tr><td colspan="6">VALUES APPLIED TO TOP 0.5 m ONLY</td><td colspan="2">VALUE APPLIED TO FULL BANK OR BAR HEIGHT</td></tr>
<tr><td rowspan="2">Factor increase in Tc value</td><td>1.10</td><td>2.00</td><td>1.10</td><td>2.00</td><td>5.00</td><td>10.0</td><td>2.00</td><td>5.00</td></tr>
<tr><td colspan="6">VALUES APPLIED TO TOP 0.5 m ONLY</td><td colspan="2">VALUE APPLIED TO FULL BANK OR BAR HEIGHT</td></tr>
</table>

4.4 BSTEM Dynamic Model Results with Vegetation

The BSTEM Dynamic runs with vegetation added to the bank and bar edges, predicted that roots do affect both the geotechnical and hydraulic processes occurring at the channel margins. The magnitude of the effects varied by species as would be expected through modeling of a range of root densities, rooting depths, and root-reinforcement values. The root-reinforcement values used in this modeling study were derived completely from field data collected along the Central Platte., As discussed in 4.3.1, however, the modification of τ_c values by roots was estimated based on the root densities measured in the field, combined with literature values for τ_c modification. As such, although actual volumes of erosion are given in Table 4-5, because of the uncertainty that exists in estimating the effects of τ_c with changing root density, it is perhaps better to compare the relative differences between the vegetated runs calibration runs, through percentage change (Table 4-5).

At the bar edges, the percent difference between calibration and vegetation runs ranged from -5.02% to 99.2% (Table 4-5), indicating that the addition of vegetation dramatically reduced the volumes of erosion predicted in some cases. At the bank edges, the presence of roots resulted in a 0 to 100% reduction in erosion volumes. It is noticeable in Table 4-5 that in the bank edge runs the differences between the Phragmites runs and the other vegetation runs, were much more distinct, preventing most or all of the erosion at the three bank sites, regardless of the rooting density.

It is interesting to note that in some cases there was actually more erosion compared to the calibration run with no vegetation when root-reinforcement and/or τ_c were increased to account for roots. This can be seen, for example, in Table 4-5, where for site XS13-2 there was more erosion for the RCG max rooting density run, than for the RCG minimum rooting density run. This result may at first seem counter-intuitive, but there is an explanation; in model runs where the upper layers were reinforced by more roots, the material could resist more undercutting, but once the driving forces acting on the upper layer exceeded the resisting forces, geotechnical failures of a larger volume then resulted. This process, along with differences between the species, and specific site details will be discussed in more detail in the following sections.

Table 4-5 Values of modeled eroded volumes, per meter of bar/bank edge, from May 2011 to Aug 2011 at the study locations, under various vegetation scenarios. Red numbers indicate model runs where more erosion was predicted compared to the calibration run.

XS 2-3 BAR			**XS 2-6 BANK**		
Vegetation Treatment	Volume eroded (m^3)	% change from calibration run	Vegetation Treatment	Volume eroded (m^3)	% change from calibration run
CW1 min	4.08	-4.62	CW1 min	0.55	0
CW1 max	2.48	36.4	CW1 max	0.55	0
CW2 min	4.08	-4.62	CW2 min	0.55	0
CW2 max	2.49	36.2	CW2 max	0.55	0
RCG min	3.37	13.6	RCG min	0.55	0
RCG max	2.45	37.2	RCG max	0.55	0
PHRAG min	0.98	74.9	PHRAG min	0	100
PHRAG max	0.19	95.1	PHRAG max	0	100

XS 13-2 BAR			**XS 13-6 BANK**		
Vegetation Treatment	Volume eroded (m^3)	% change from calibration run	Vegetation Treatment	Volume eroded (m^3)	% change from calibration run
CW1 min	28.4	-4.41	CW1 min	0.09	0
CW1 max	26.4	2.94	CW1 max	0.09	0
CW2 min	28.4	-4.41	CW2 min	0.09	0
CW2 max	23.5	13.6	CW2 max	0.09	0
RCG min	26.9	1.10	RCG min	0.09	0
RCG max	32.3	-18.8	RCG max	0.09	0
PHRAG min	1.41	94.8	PHRAG min	0	100
PHRAG max	0.207	99.2	PHRAG max	0	100

XS 20-6 BAR			**XS 20-7 BANK**		
Vegetation Treatment	Volume eroded (m^3)	% change from calibration run	Vegetation Treatment	Volume eroded (m^3)	% change from calibration run
CW1 min	20.5	-5.02	CW1 min	1.3	5.80
CW1 max	18.2	6.76	CW1 max	1.3	5.80
CW2 min	20.5	-5.02	CW2 min	1.3	5.80
CW2 max	16.0	18.0	CW2 max	1.07	22.5
RCG min	10.2	47.7	RCG min	1.21	12.3
RCG max	14.1	27.8	RCG max	1.19	13.8
PHRAG min	9.41	51.8	PHRAG min	0.05	96.4
PHRAG max	0.182	99.1	PHRAG max	0.0008	99.9

4.4.2 Cottonwood

For the XS2-3 bar site (Figure 4-3a), the CW1 min and CW2 min runs resulted in a similar erosion profile to the calibration run with no vegetation. In fact, the volume eroded was approximately 4.6% more than in the calibration run (Table 4-5). This is because the slight increase in hydraulic resistance of the upper layer led to preferential erosion of the bottom layer of the bar, resulting in slightly more undercutting than in the calibration run. Because the root-reinforcement in the CW1 min and CW2 min runs was negligible, there was not enough cohesion in the upper bar material to prevent geotechnical failures once undercutting had taken place. In the CW1 max and CW2 max runs, again, preferential undercutting of the bottom layer occurred because the upper layer had a higher τ_c value than the lower layer to account for the presence of roots. In these runs, however, the increased root-reinforcement (0.69 and 2.36 kPa for CW1 max and CW2 max runs, respectively) was sufficient to prevent as many geotechnical failures from occurring, and overall erosion was approximately 36% less than the calibration run for both CW1 max and CW2 max.

Similar results were seen for the bar edges at sites XS13-2 and XS20-6 (Figures 4-4a and 4-5 a), but at both of these sites the difference between the CW1 max and CW2 max runs was greater than at siteXS2-3. At XS13-2 the CW1 max run showed an eroded volume that was approximately 3% less than the calibration run, but the additional root-reinforcement provided by an additional year of growth, resulted in an eroded volume 13.6 % less than the calibration run. At XS20-6, the CW1 max run resulted in a 6.76 % reduction in eroded volume, compared to an 18.0 % reduction for the CW2 max model run.

This larger difference between the CW1 and CW2 maximum rooting density runs at XS13-2 and XS20-6, compared to site XS2-3, was a function of the higher bar heights at these two sites. As bar height increased, the un-reinforced lower layer underpinning the 0.5 m deep reinforced upper layer, became thicker, allowing for more undercutting, and increasing the importance of the resistance to geotechnical failure provided by roots in the upper layer.

At the bank edge sites (Figure 4-3b, 4-4b and 4-5b), the addition of cottonwood seedlings to the model runs provided little to no change in eroded volumes, largely as a result of their low rooting density. At sites XS2-6 and XS13-6, no difference was seen compared to the calibration runs. At site XS20-7 the CW2 max run produced a 22.5% reduction in eroded volume compared to the calibration run, but overall eroded volumes were still small.

a)

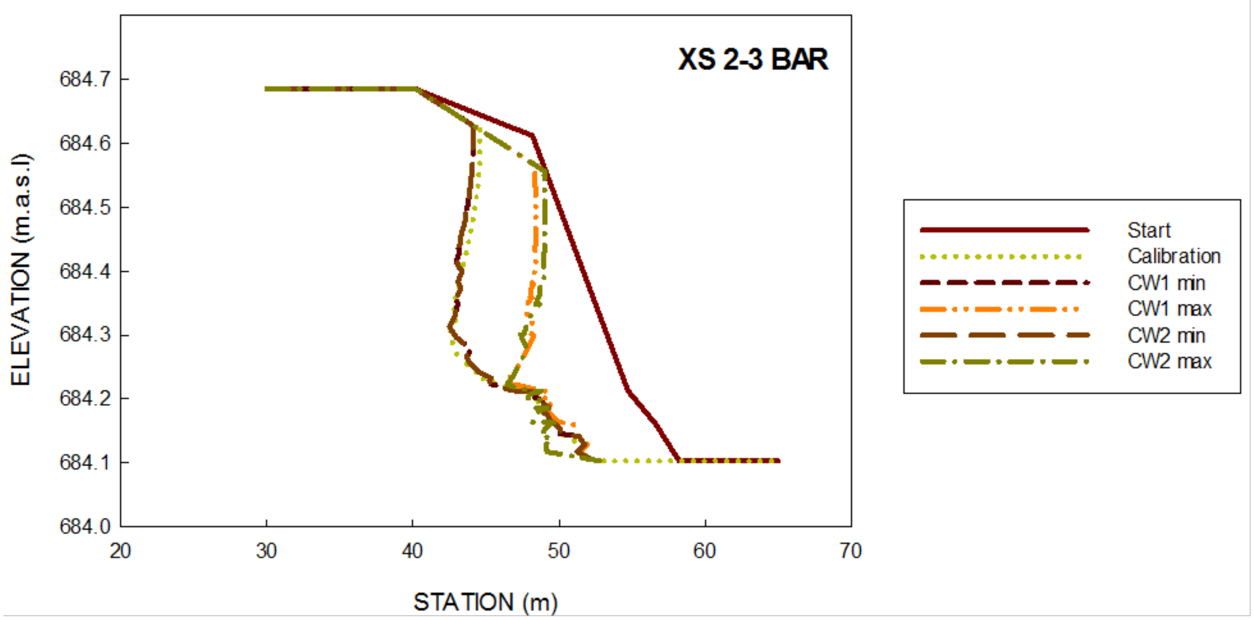

b)

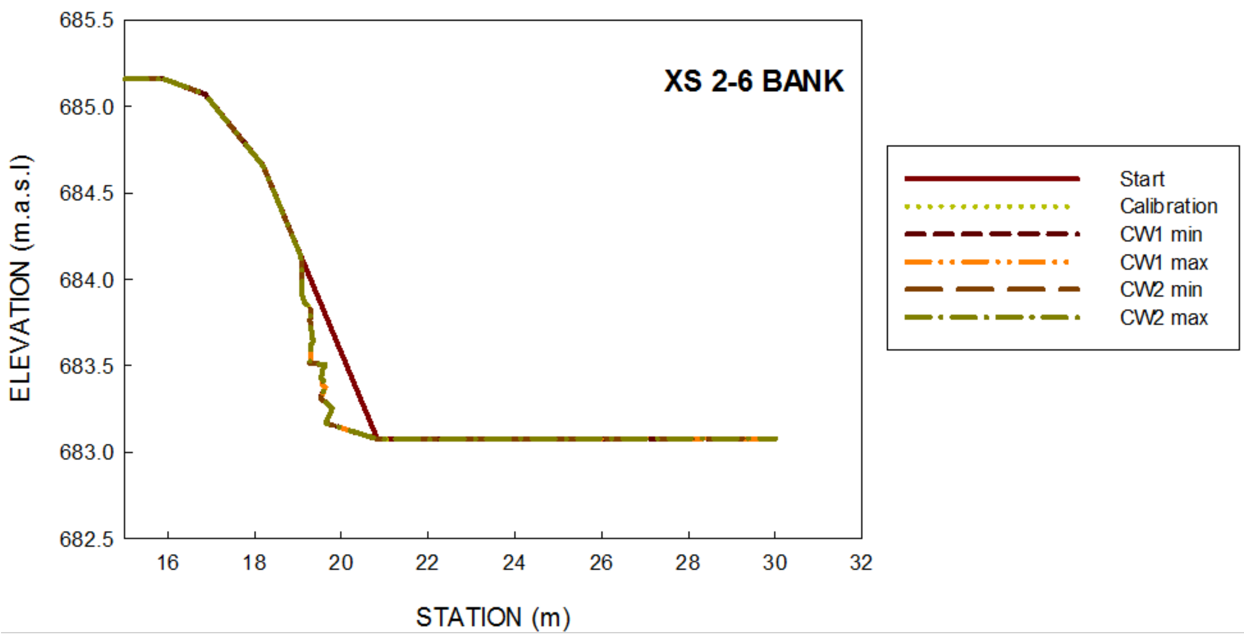

Figure 4-3 Before and after bar- and bank- edge profiles from BSTEM Dynamic runs compared to the calibration runs at a) XS2-3 and b) XS2-6 with cottonwood seedlings.

a)

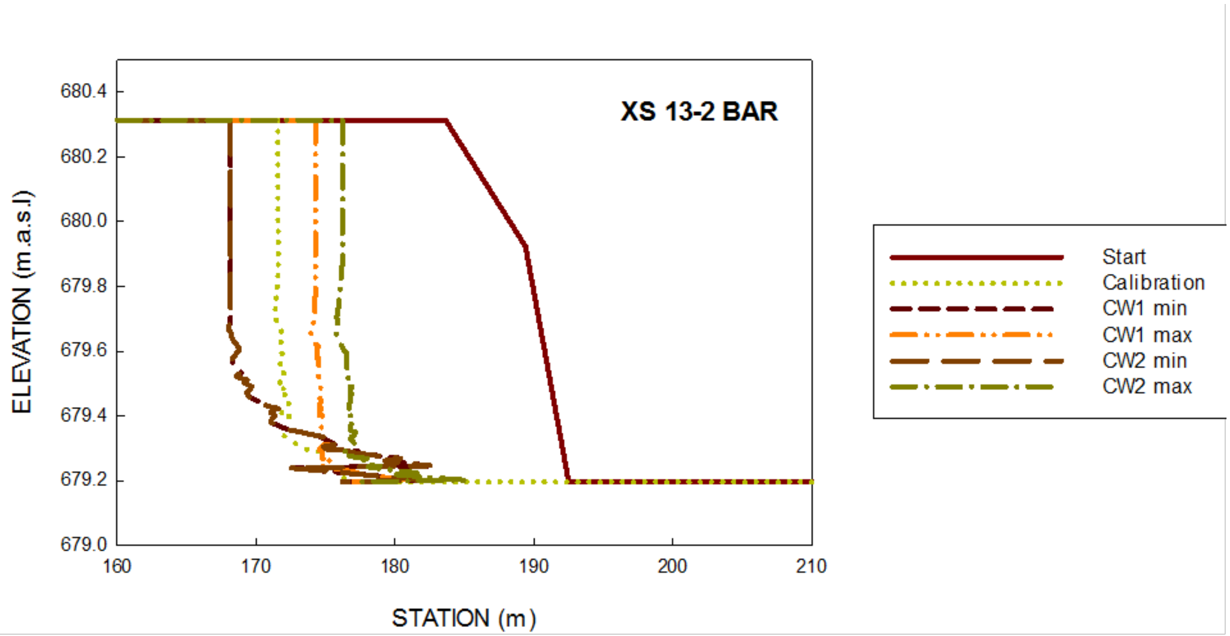

b)

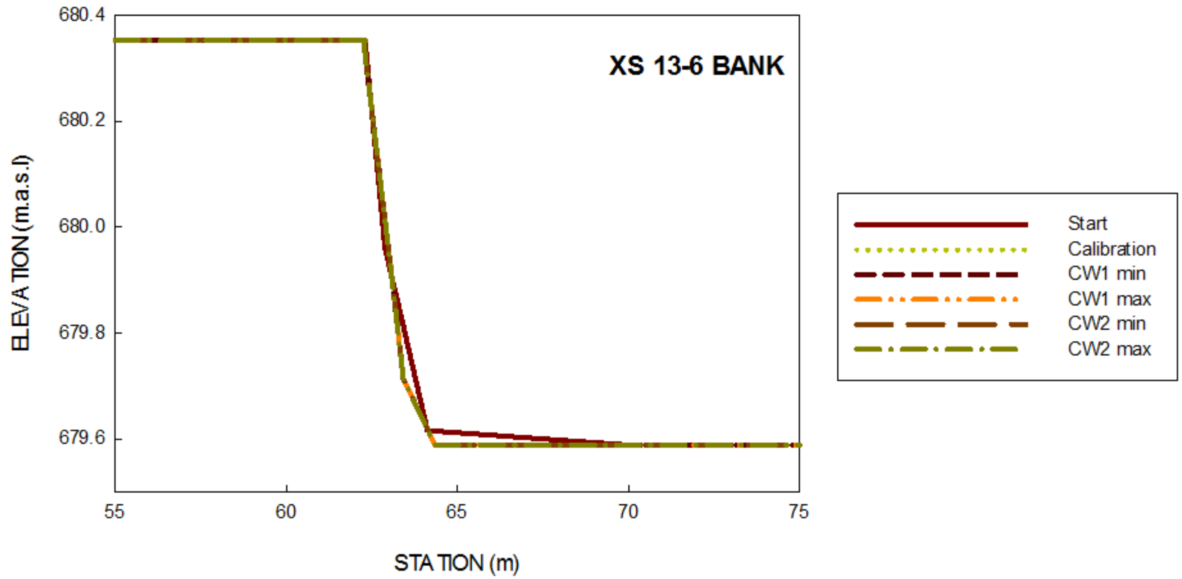

Figure 4-4 Before and after bar- and bank- edge profiles from BSTEM Dynamic runs compared to the calibration runs at a) XS13-2 and b) XS13-6 with cottonwood seedlings.

a)

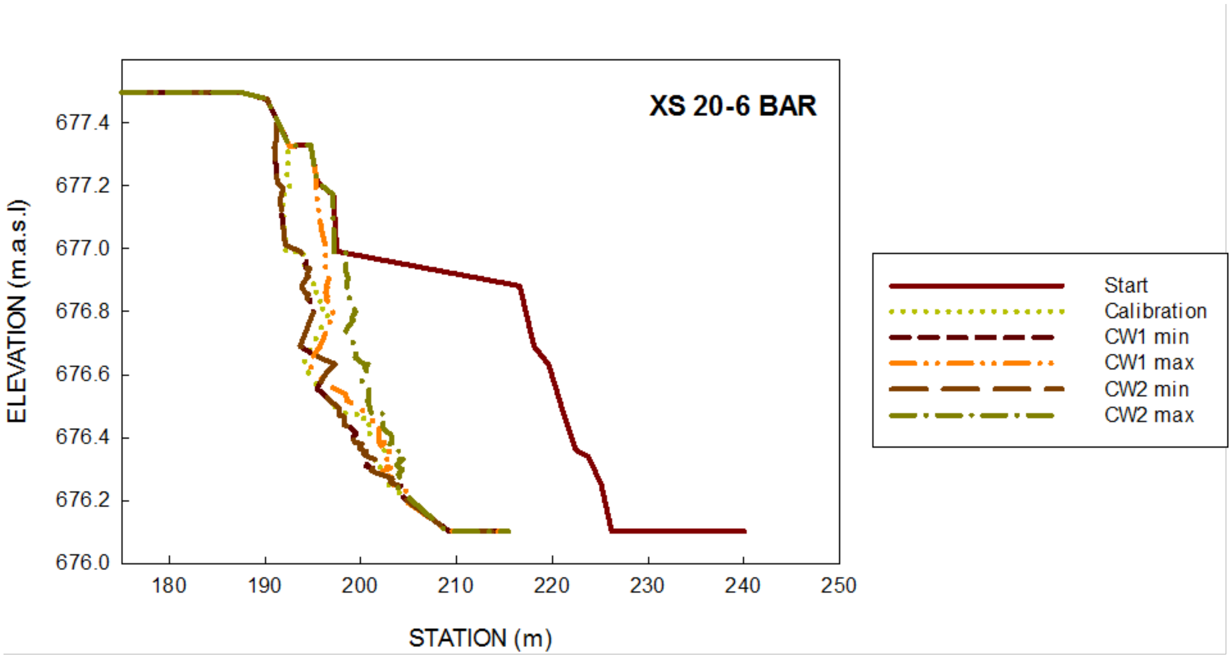

b)

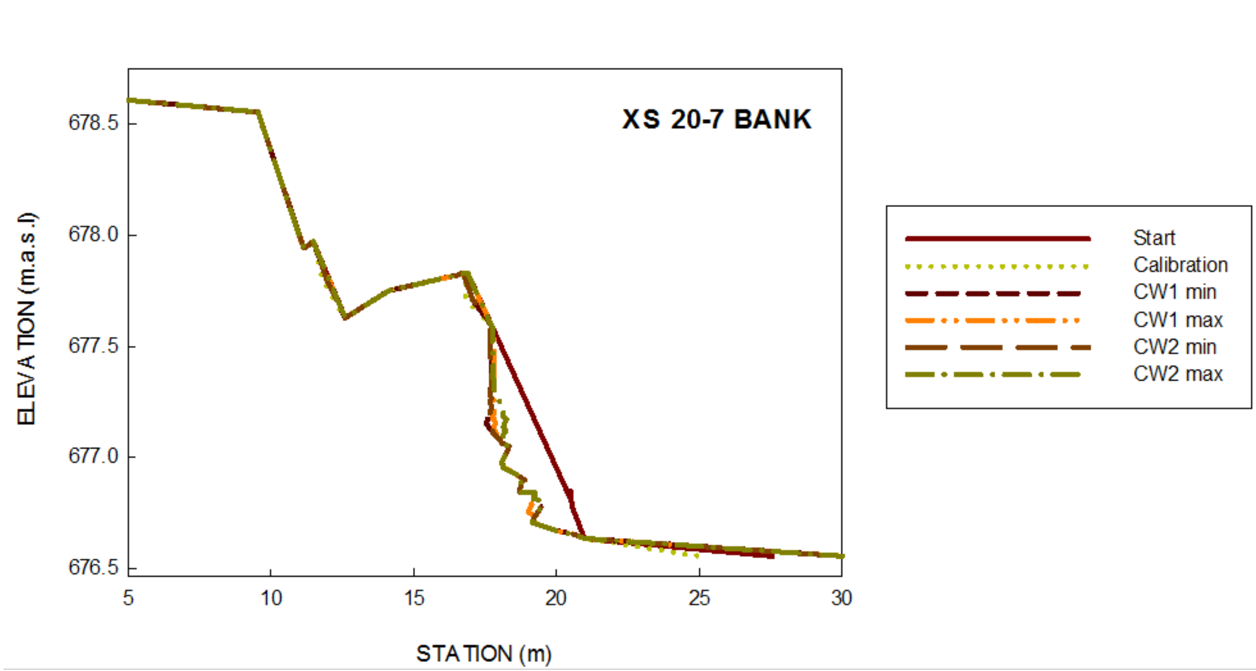

Figure 4-5 Before and after bar- and bank- edge profiles from BSTEM Dynamic runs compared to the calibration runs at a) XS20-6 and b) XS20-7 with cottonwood seedlings.

4.4.3 Reed canarygrass

Model results for Reed canarygrass showed complex responses to the reinforcement of the upper 0.5m of bar or bank by the dense networks of roots. At site XS2-3, the shortest bar modeled, BSTEM predicted that with Reed canarygrass present at the bar edge, the eroded volume over the study period would have been 13.6 to 37.2 % less than the calibration run with no vegetation (Figure 4-6a). At this site the run with greater root-reinforcement (RCG max) correspondingly predicted less erosion than the run with lower root-reinforcement (RCG min).

4.4.3.1 Bar Edges

At the taller bar edge sites, XS13-2 and XS20-6, a greater volume of erosion was seen under in the higher rooting density model run, RCG max, than in the lower rooting density run, RCG min. As with the cottonwood runs discussed in the previous section, the rooting depth to total bar or bank height was particularly important in these runs; in the runs with a taller bar, a deeper un-reinforced lower layer was present, allowing for greater undercutting of the reinforced upper layer. In these two cases, the higher the root-reinforcement of the upper layer, the greater the resistance to geotechnical failure, and the more undercutting could be withstood. Once the driving forces had overcome the resisting forces, however, a larger failure volume resulted. This explains why the eroded volume was greater in the RCG max runs than the RCG min runs at two of the bar edge locations. At site XS13-2 (Figurue 4-7a) the geometry of the bar edge was such that geotechnical failures following undercutting of the root mat of the Reed canarygrass, resulted in eroded volumes that were up to 18.8% greater than the calibration run without vegetation. At site XS20-6, the initial bar geometry had a stepped profile (Figure 4-8a), so more undercutting had to take place before the upper reinforced layer became undercut. As a result, at this location, the volume of erosion with Reed canarygrass present at the bar edge was 27.7 to 47.8 % less than the calibration run.

A range of different yet systematic outcomes were seen for these bar edge model runs with Reed canarygrass, depending on the rooting depth to bar height ratio, undercutting of the reinforced root layer, and resulting geotechnical failure volumes.

4.4.3.2 Bank Edges

At the bank edge sites, XS2-6, and XS13-6 (Figures 4-6b and 4-7b respectively), the volumes of erosion with Reed canarygrass were the same as for the calibration run with no vegetation. At site XS20-7 (Figure 4-8b) the roots in the upper layer prevented a small area of the stepped bank profile from eroding, resulting in 12.3 to 13.8 % less erosion compared to the calibration run.

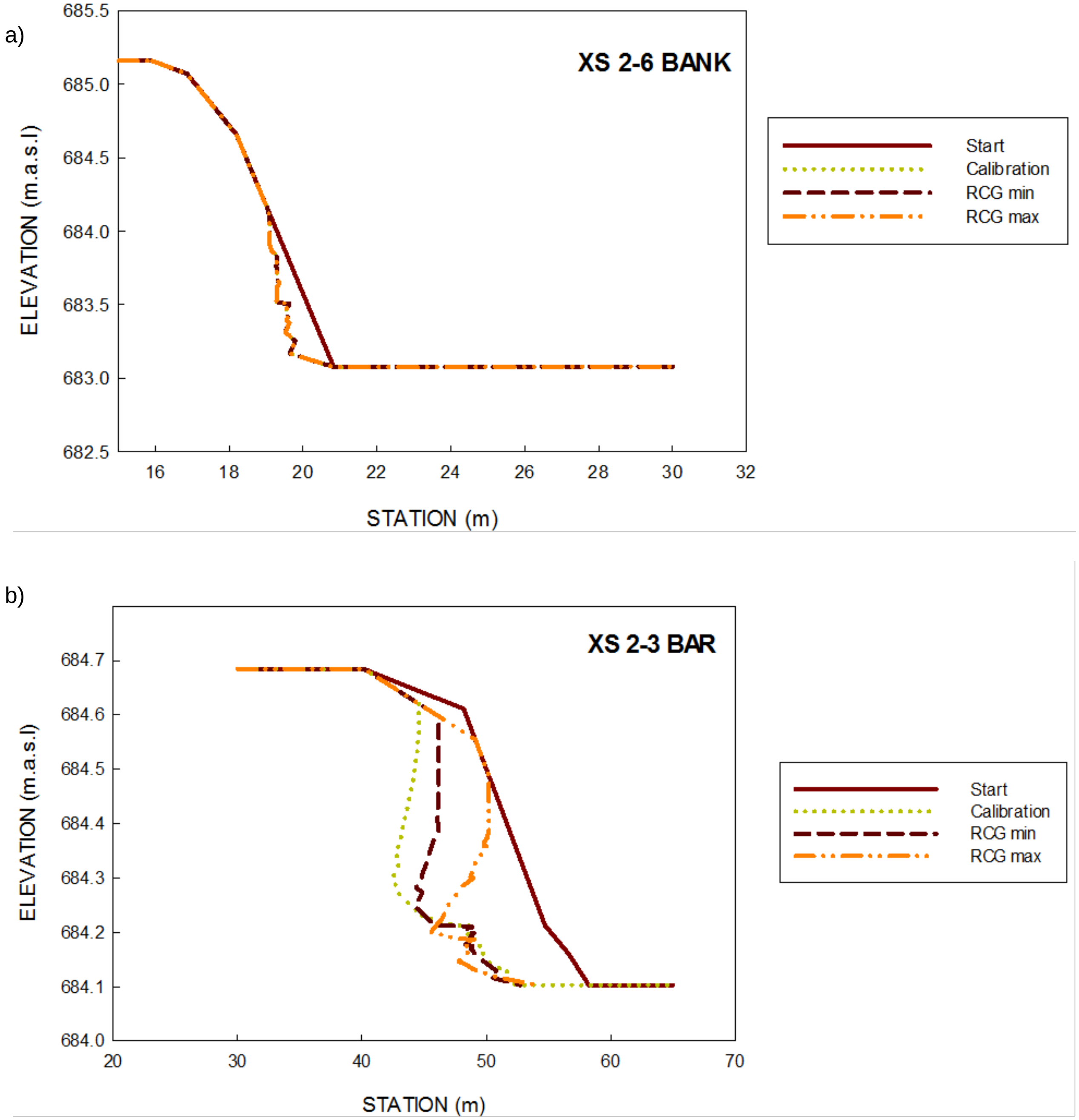

Figure 4-6 Before and after bar- and bank- edge profiles from BSTEM Dynamic runs compared to the calibration runs at a) XS2-3 and b) XS2-6 with Reed canarygrass.

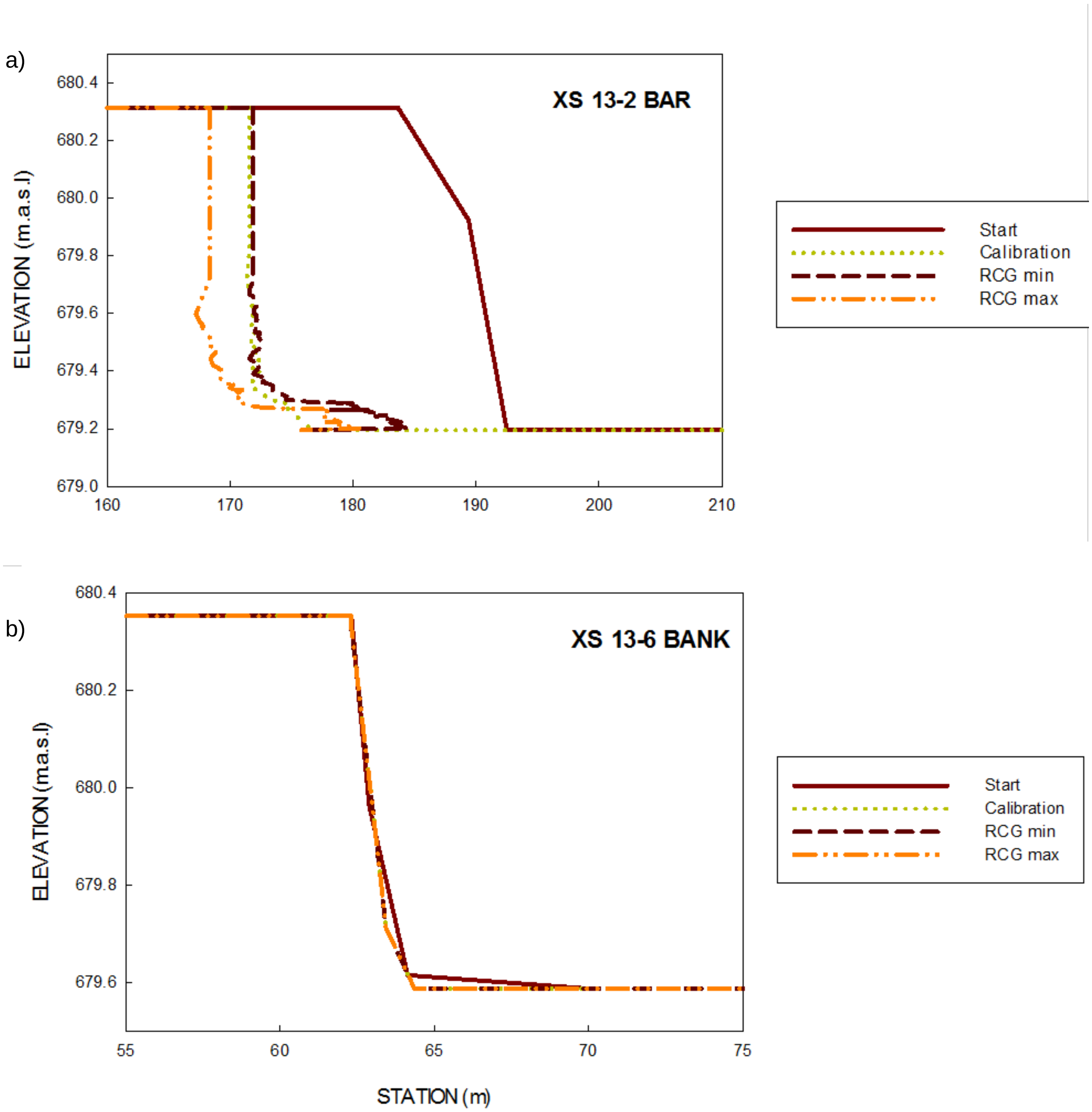

Figure 4-7 Before and after bar- and bank- edge profiles from BSTEM Dynamic runs compared to the calibration runs at a) XS13-2 and b) XS13-6 with Reed canarygrass.

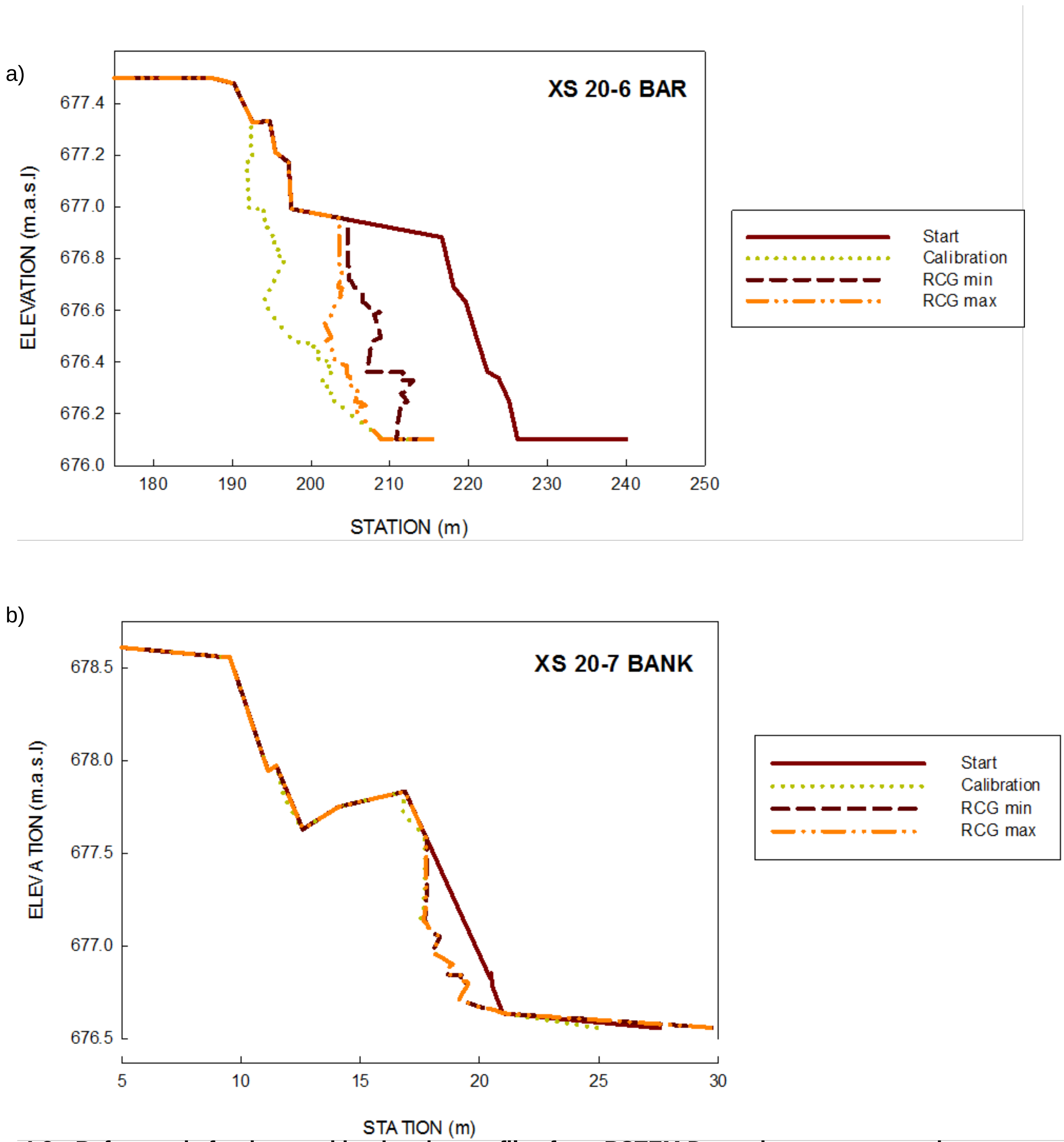

Figure 4-8 Before and after bar- and bank- edge profiles from BSTEM Dynamic runs compared to the calibration runs at a) XS20-6 and b) XS20-7 with Reed canarygrass.

4.4.4 Phragmites

In the BSTEM runs involving *Phragmites*, the modified input parameters were applied to the entire bar or bank height. Because of this, both layers of the bar/bank eroded at the same rate, and undercutting of the reinforced upper layer was not a factor. The resulting profiles were, therefore, less complex than the runs for cottonwood and Reed canarygrass, again highlighting the importance of the rooting depth to bar/bank height ratio.

In all cases, the runs with *Phragmite*s predicted less erosion than the calibration run, and less erosion was predicted in the PHRAG max runs compared to the PHRAG min runs. At site XS2-3 (Figure 4-9a) the presence of *Phragmites* at the bar edge reduced erosion by 74.9 to 95.1 %. At site XS13-2 (Figure 4-10a) erosion was reduced by 94.8 to 99.2 %, and at site XS20-6 (Figure 4-11a) erosion was reduced by 51.8 to 99.1 %. At the minimum root-reinforcement value modeled for *Phragmites*, considerable volumes of lateral bar erosion, therefore, still occurred, albeit in smaller volumes than those predicted in the cottonwood and Reed canarygrass runs. At the maximum root-reinforcement value modeled, *Phragmites* dramatically reduced erosion volumes at the bar edges, but even at this maximum root-reinforcement value (42.0 kPa in the PHRAG max runs), a small amount of hydraulic erosion still occurred.

At the bank edges, the model runs predicted that the presence of *Phragmites* prevented any erosion from occurring at sites XS2-6 and XS13-6 (Figures 4-9b and 4-10b respectively) and reduced erosion by 96.4 to 99.9% at site XS20-7 (Figure 4-11b). As with the other runs for bank edges, eroded volumes in these runs were much smaller than those at the bar edges.

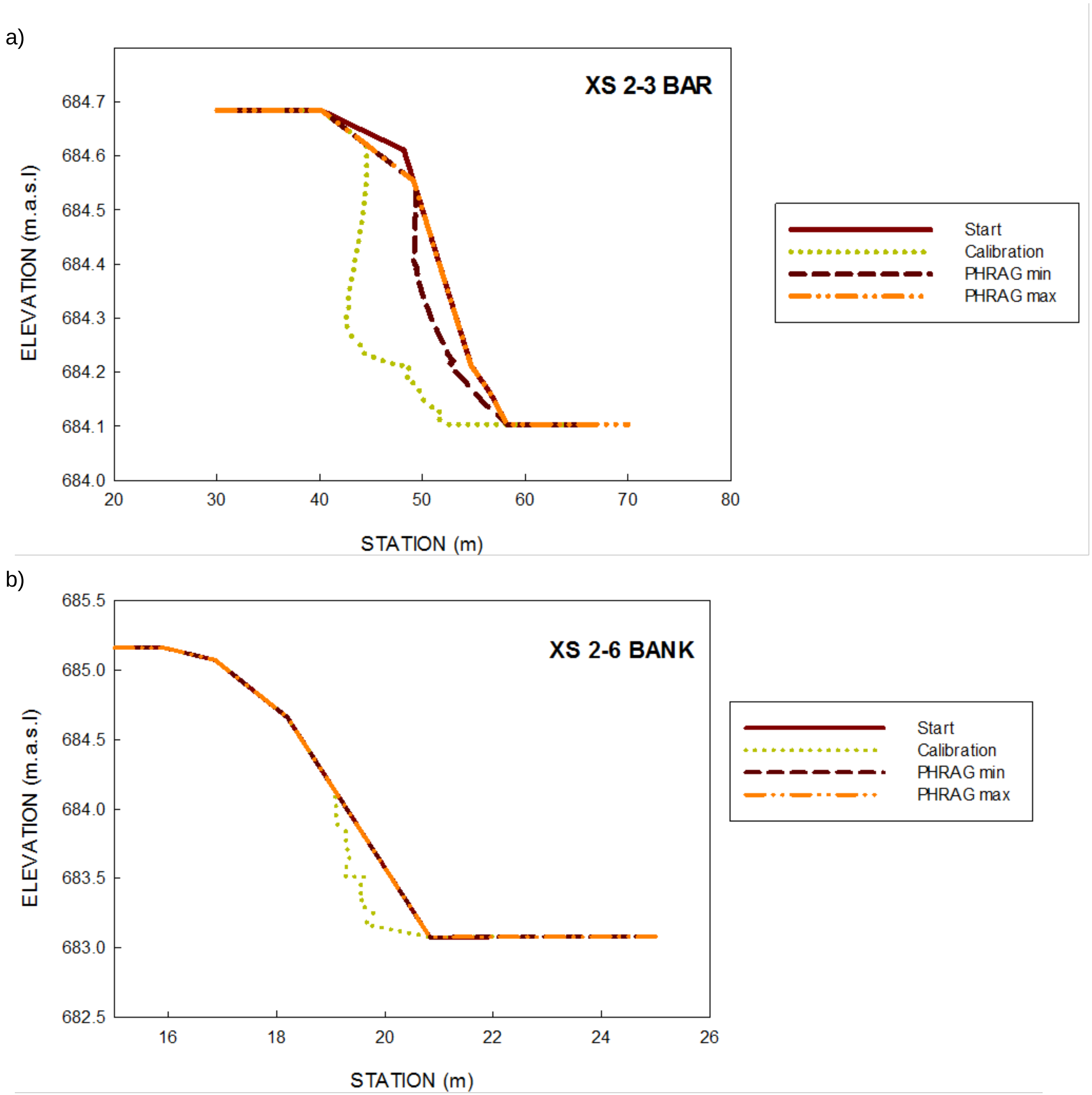

Figure 4-9 Before and after bar- and bank- edge profiles from BSTEM Dynamic runs compared to the calibration runs at a) XS2-3 and b) XS2-6 with *Phragmites*.

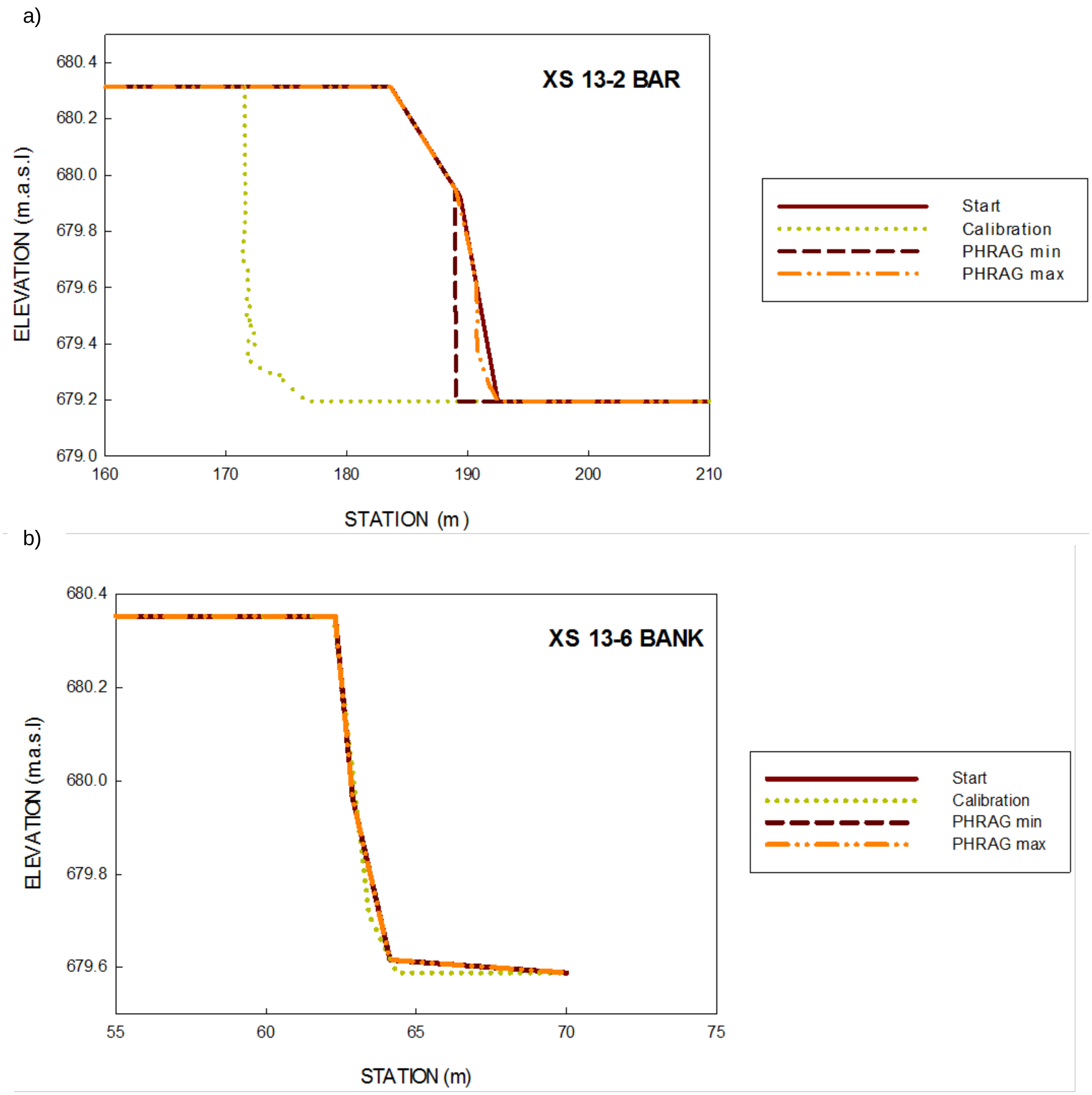

Figure 4-10 Before and after bar- and bank- edge profiles from BSTEM Dynamic runs compared to the calibration runs at a) XS13-2 and b) XS13-6 with *Phragmites*.

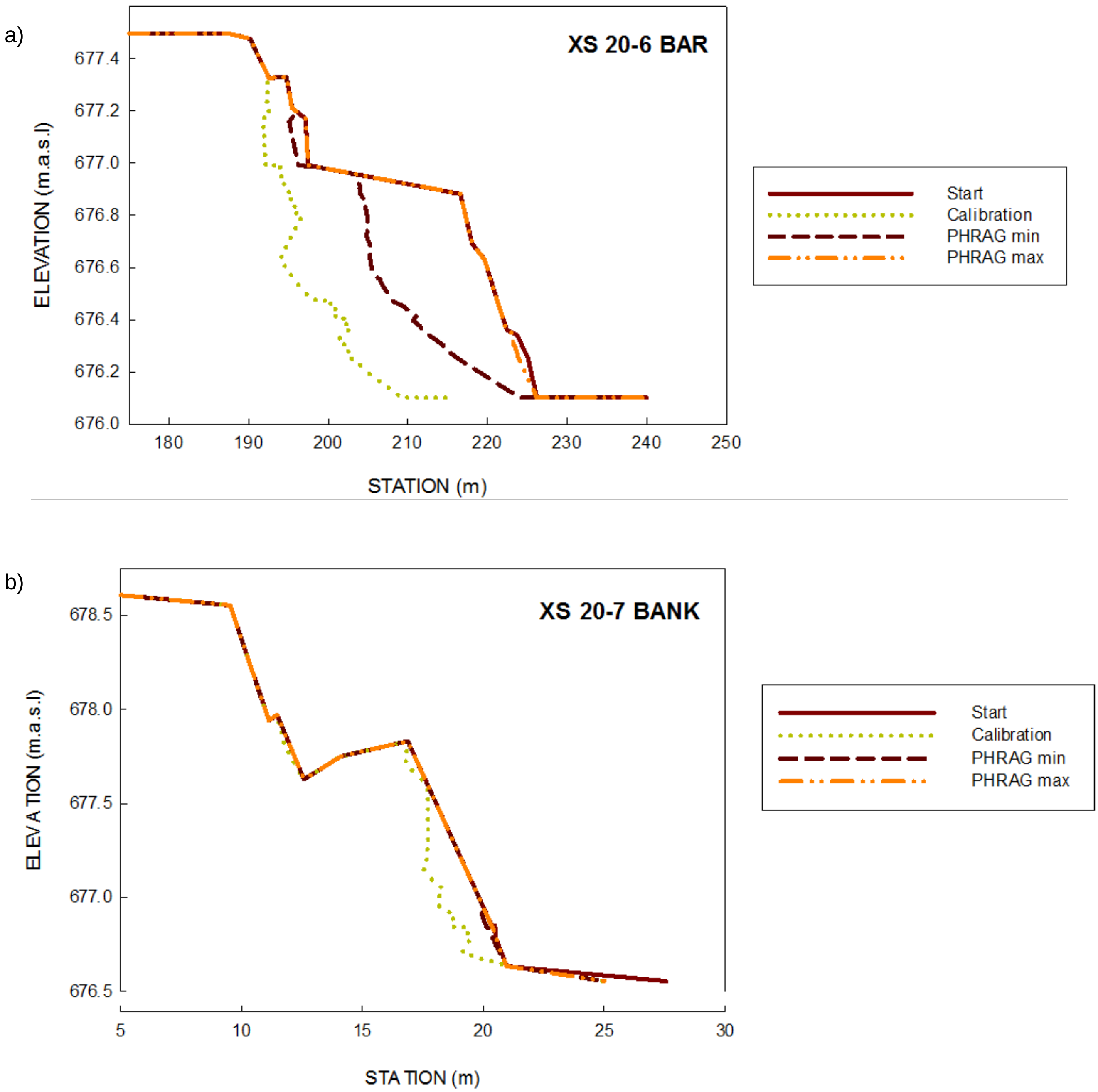

Figure 4-11 Before and after bar- and bank- edge profiles from BSTEM Dynamic runs compared to the calibration runs at a) XS20-6 and b) XS20-7 with *Phragmites*.

In summary, for each species, the rooting depth to bar height ratio, along with root strength and density affect the amount of undercutting that occurs at a given bar edge. These factors also control the depth of undercut that can be withstood before a geotechnical failure occurs (Figure 4-12). The interplay between these factors can lead to complex patterns of bar edge erosion, and bar retreat rates, as seen in the model results discussed previously.

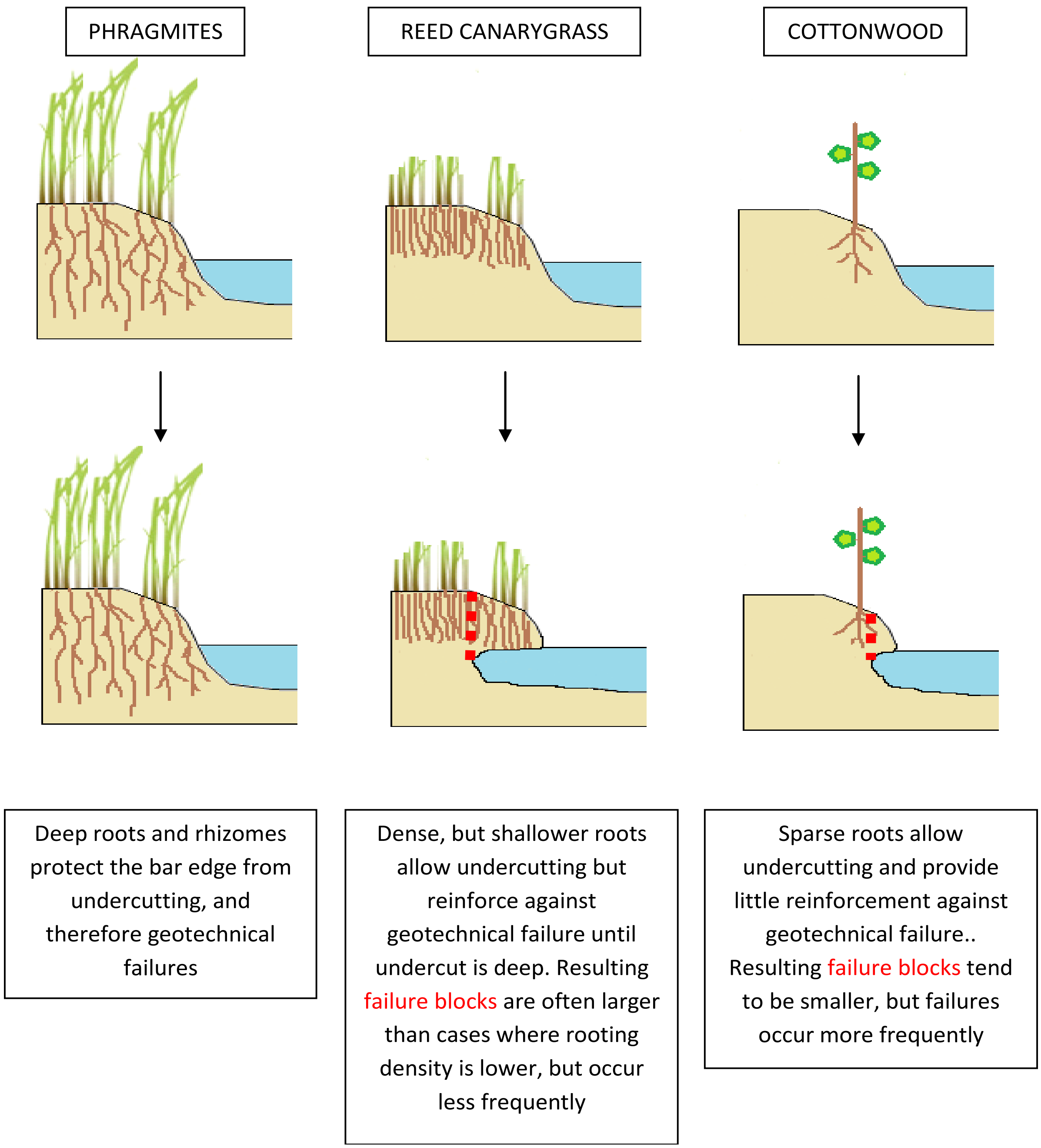

Figure 4-12 Illustration of how rooting depth and density affect extent of undercutting and resulting geotechnical failures.

4.5 Effects of low flows and SDHFs on timing and magnitudes of geotechnical and hydraulic erosion at bank and bar edges

One of the sub-objectives of this study was to look at the timing of erosion at bar edges in relation to stage and discharge. This analysis will help PRRIP to assess the use of SDHFs as a tool for vegetation management as part of their overall Flow-Sediment-Mechanical (FSM) approach. To examine the effect of variations in discharge on erosion volumes, one site was selected for more detailed investigation, the bar edge location XS2-3. Daily output from BSTEM for hydraulic and geotechnical erosion volumes were plotted along with discharge for the modeled time period (Figures 4-12 to 4-14). In addition, the contribution to total eroded volume from hydraulic versus geotechnical erosion was plotted for each model run (Figure 4-15).

In the cottonwood runs in Figure 4-12, it can be seen that hydraulic erosion occurs in almost every time step during the three month model run. This is because the bar material had a low critical shear stress (particularly in the layer below the root zone), allowing for entrainment even at lower discharge values, such as those during the first month of the model run which never exceeded 4,000 ft^3s^{-1}. In fact, the plots show that daily volumes of hydraulic erosion were higher at the onset of the model run, as the toe was eroded and the bar edge was steepened. Eroded volumes from hydraulic erosion were less during the higher flow events because the bank geometry had been changed through earlier erosion, and the distribution of shear stresses at the bar edge, thus changed.

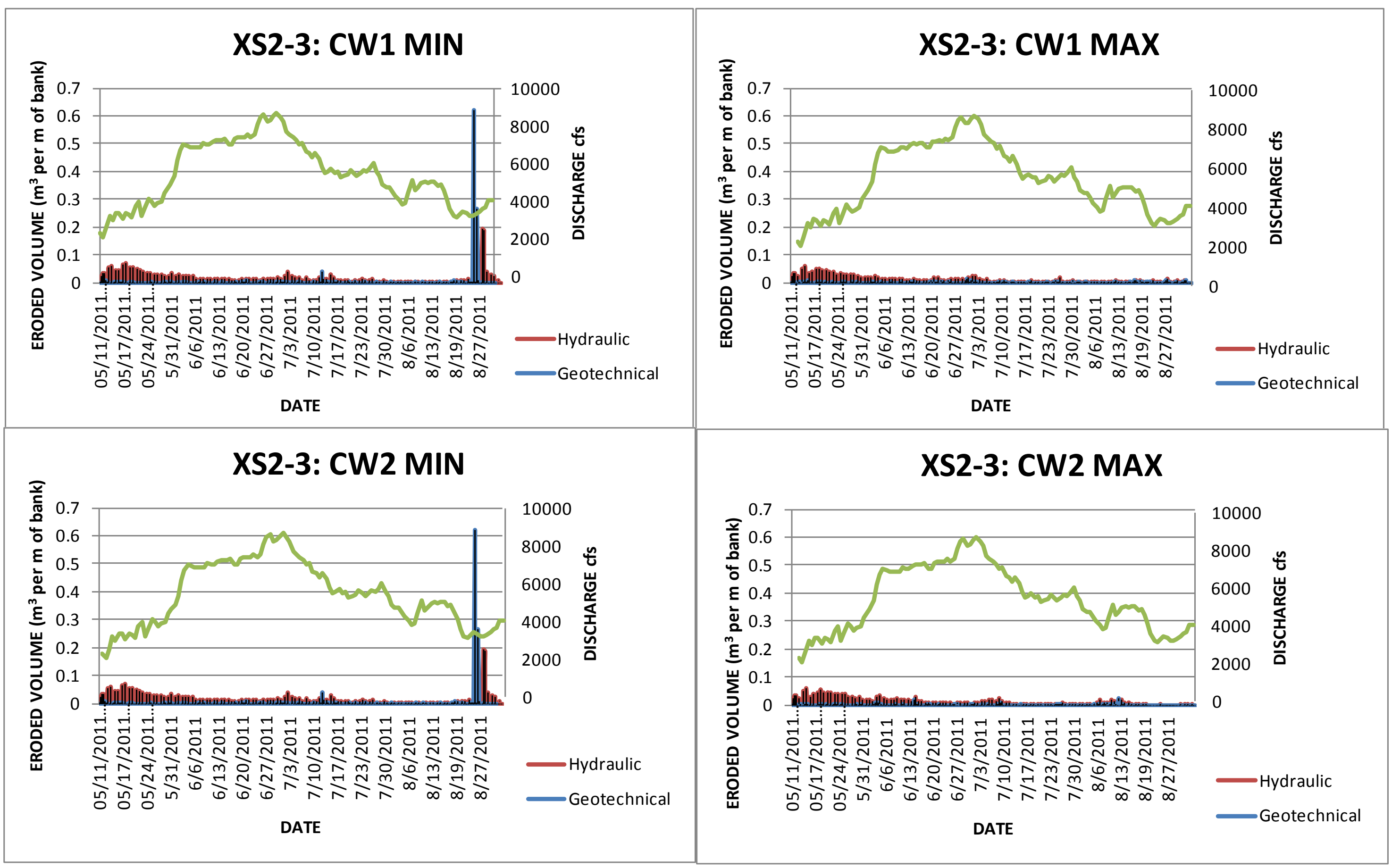

Figure 4-13 Timing and magnitude of hydraulic and geotechnical erosion over the period modeled in BSTEM, for CW1 and CW2 scenarios.

In the CW1 min and CW2 min runs, two large geotechnical failure events can be seen in the model output: July 10th, and August 24th. These two events did not correspond to periods of high discharge or even drawdown after high discharge, which is typically the most common time for geotechnical failures to occur as bank/bar saturation is high and confining force from the flow is low. Instead, geotechnical failures occurred when undercutting at the base of the bank created a situation where the driving forces acting on the bank exceeded the resisting forces. In this case, this resulted from prolonged low magnitude hydraulic erosion throughout the entire range of discharges that the bar edge was exposed to. The largest, most significant geotechnical failure therefore occurred near the end of the model run. In the CW1 max and CW2 max runs, the same volumes of daily hydraulic erosion can be seen in the plots in Figure 4-12, but the root-reinforcement in the upper bar layer prevented the large geotechnical failure occurring towards the end of the model run. In both the CW min and CW max runs, small geotechnical failures also occurred throughout the entire modeling period as a result of undercutting and geotechnical failures of small volumes of the bar face. A longer model run would likely produce sufficient undercutting in the CW 1 max and CW2 max runs to also cause a large geotechnical failure such as that seen in the CW min runs. The greater the root-reinforcement in the upper layer, the more undercutting, and longer flow duration required to produce a large geotechnical failure. The results for cottonwood therefore suggest, that geotechnical failures will occur at all rooting densities in the cottonwood seedling age range up to two years, but the frequency and magnitude of those failures will decrease as root systems become denser and deeper. Figure 4-15 shows that hydraulic erosion dominated the CW runs.

The RCG min run at XS2-3 showed a similar pattern of hydraulic erosion and undercutting of the upper root-reinforced layer, followed by two larger geotechnical failures towards the end of the RCG min model run and one towards the end of the RCG max run. The timing of the major geotechnical failures in these runs, however, corresponded to a drawdown condition, when discharge decreased rapidly, leaving the bar material saturated and removing the confining force from the flow. Slightly less hydraulic erosion occurred in the RCG min run compared to the CW min runs (Figure 4-15), but this erosion was focused more on undercutting of the lower layer, because the τ_c of the upper layer was higher in the RCG runs compared to the CW runs, and therefore resisted as much hydraulic erosion. The undercut remained stable while flows were high, because of the confining force from the flow. However, once that confining force was removed, the driving forces exceeded the resisting forces of the bar, and a larger geotechnical failure occurred compared to the CW runs, because the depth of the undercut was greater.

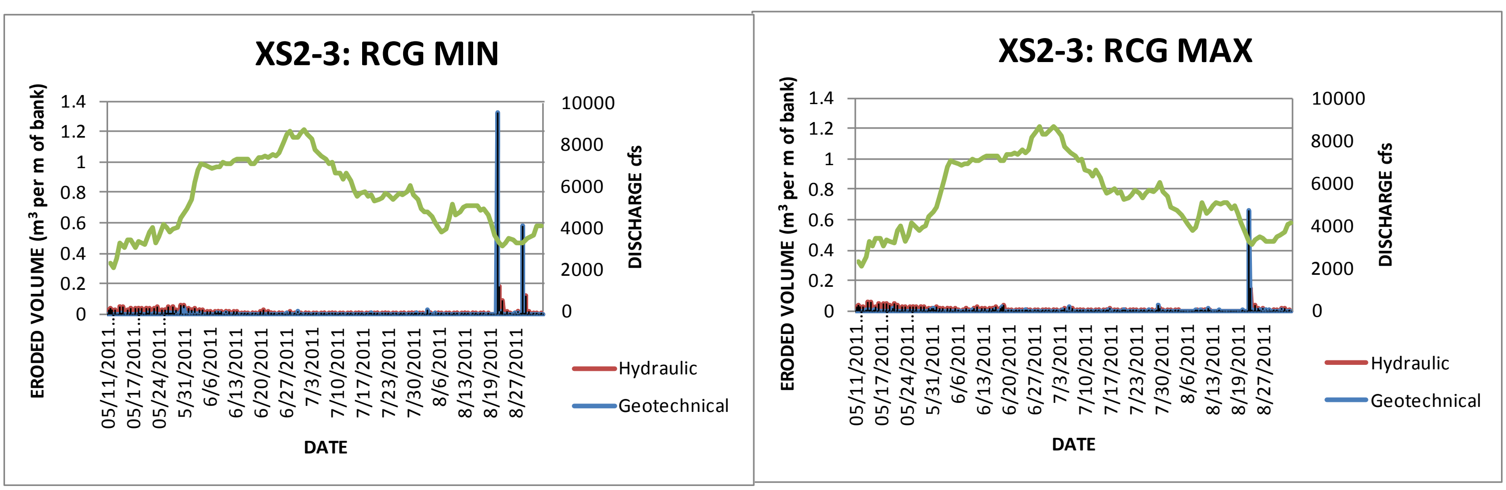

Figure 4-14 Timing and magnitude of hydraulic and geotechnical erosion over the period modeled in BSTEM, for RCG scenarios.

The *Phragmites* model runs at XS2-3 showed that small volumes of hydraulic erosion and geotechnical erosion occurred throughout the PHRAG min run (Figure 4-14). Even though the entire bar height was reinforced with roots in this run, the rooting density at the lower end of the spectrum for *Phragmites* was insufficient to prevent all erosion from occurring. No major geotechnical failures occurred, however, and hydraulic erosion dominated what little erosion did take place (Figure 4-15). In the PHRAG max run, the reinforcement throughout the bar by dense rhizomes and roots, prevented any geotechnical failures or hydraulic erosion during the period modeled, even up to discharge values greater than 8,000 ft^3s^{-1}.

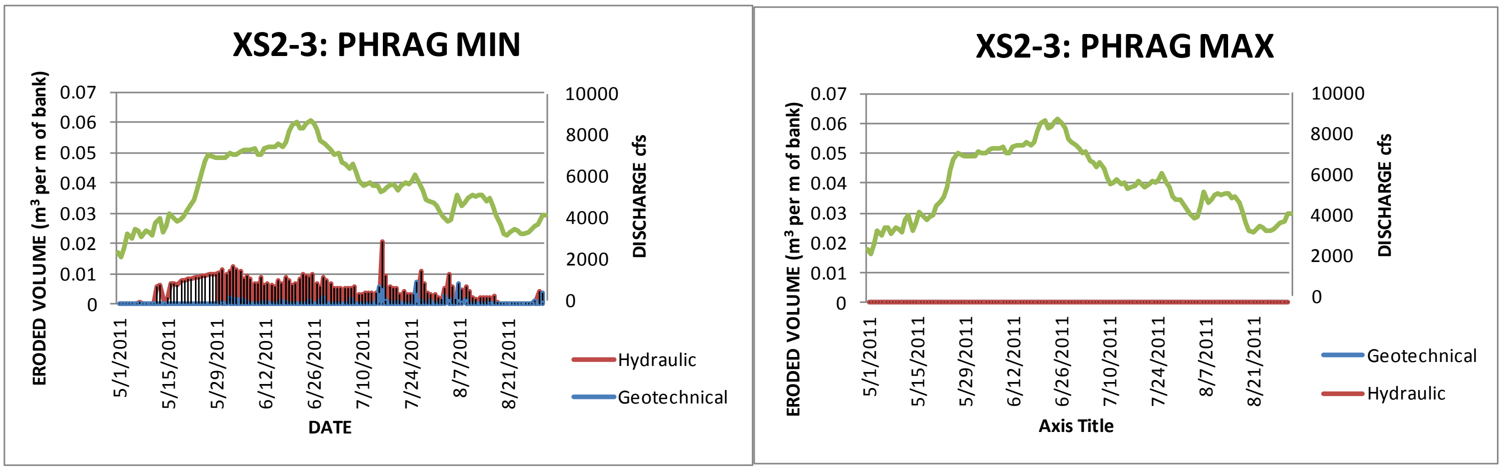

Figure 4-15 Timing and magnitude of hydraulic and geotechnical erosion over the period modeled in BSTEM, for *Phragmites* scenarios.

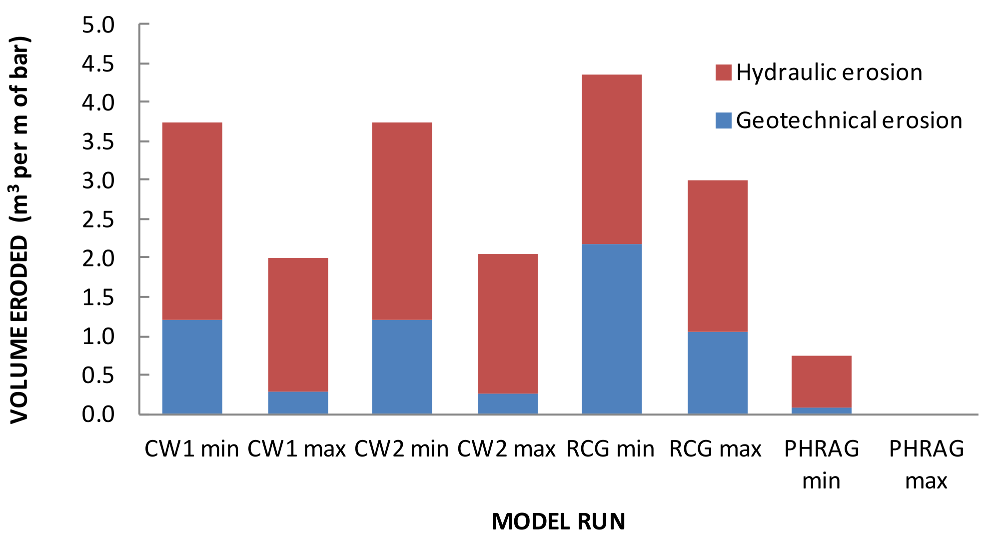

Figure 4-16 Volumes of hydraulic versus geotechnical erosion in each model run.

This section highlights, that the timing and magnitude of geotechnical failure events were largely a function of the magnitude of root-reinforcement of the upper layer of the bar (through increased critical shear stress and shear strength due to roots) and their effects on location/focus of hydraulic erosion, and the amount of undercutting required for the resisting forces to be overcome. The daily erosion plots also showed that the low cohesion, sandy materials that make up the bars of the Central Platte River, are easily entrained, at the margins under a wide range of discharges, not just during SDHF events. As a result, a long period of exposure to continual hydraulic erosion can still result in geotechnical failures of the bar edges under some vegetation scenarios, regardless of the occurrence of a SDHF.

4.5.2 BSTEM results for a 3-day SDHF event of 8,000 ft^3/s

To examine the effect of a SDHF as a stand-alone event, a separate model run was performed for the XS2-3 bar edge site. The SDHF modeled was a 3-day event with a discharge of 8,000 ft^3/s, with flow receding to baseflow on the fourth day, to simulate a worst case condition with a rapid drawdown of flow, and maximum potential instability at the bar edge.

The amount of erosion modeled for this four-day period was approximately 1% of the total erosion recorded in the full model run for May to August 2011. All of the eroded volume resulted from hydraulic scour, with no geotechnical erosion predicted, even during the drawdown condition. This model result highlights again, the importance of prolonged hydraulic erosion as a primer for geotechnical failures at bar edges. Had the bar edge geometry modeled been steepened and undercut to illustrate prior hydraulic erosion, a geotechnical failure during the SDHF event drawdown condition would have been far more likely. The geometry of the bank and bar edges at the onset of any planned SDHF events will thus impact the width and volume of any erosion. Rates of bank and bar erosion are therefore, not necessarily positively correlated to the size of a discharge event, as bank and bar edge retreat is a progressive, non-linear process.

5 Implications for Vegetation Management and Sediment Dynamics in the Central Platte River

The BSTEM Dynamic results presented in Chapter 4 showed that the different species of vegetation investigated in this study, had varying and sometimes quite complex effects, on the timing and magnitudes of lateral bar and bank erosion. In combination with the results presented in the first Directed Vegetation Study (Pollen-Bankhead et al., 2010), these results have implications for the longterm management of bar vegetation along the Central Platte River, resulting bar stability and sediment dynamics within the fluvial system.

5.1 Cottonwood seedlings

The BSTEM runs for cottonwood seedlings showed that erosion can still occur at bar and bank edges when these seedlings are young, rooting densities are low, and rooting depth to bar/bank height ratios are small. At this early stage of cottonwood development, the BSTEM runs suggested that SDHFs were not required for lateral erosion (that would also remove any cottonwoods growing on the bar top), to take place. This was because the low cohesion and small particle diameters (predominantly in the sand range) of the bars and banks along the Central Platte River are easily entrained. Hydraulic erosion and associated geotechnical instability occurs, therefore, at bar and bank edges under a wide range of discharges, not just during SDHF events.

Field data, numerical and physical modeling results presented by Pollen-Bankhead et al. (2010) indicated that the weakest and most shallow rooted cottonwood seedlings could be removed by drag forces acting on the stems during SDHF events. The results presented here show that young cottonwood seedlings can also be removed from bank and bar edges by lateral scour and undercutting occurring from sustained hydraulic scour at lower flow stages, in conjunction with SDHF events. The model results showed that erosion during a SDHF event of 3 days, in isolation, was not sufficient to remove these plants, and that longer periods of scour, at lower discharges are required to ‘prime’ the bar edges for failure at higher flows. The implication for management of cottonwood seedlings along the Central Platte River then, is that little management of young cottonwoods should be required, especially at lower elevations, where hydraulic scour occurs at lower discharges, and thus, for extended periods of time. Because lateral erosion was still predicted in the all of the cottonwood model runs, even under the highest root densities modeled, it is likely that those cottonwoods that do survive on bars will be located away from bar edges, and/or at elevations that are subject to shorter durations of hydraulic scour, so that roots have time to establish. Cottonwoods growing at higher bar elevations may, therefore, need to be removed mechanically if their roots become established.

Calculation of eroded volumes and percent difference compared to the calibration runs, showed that the presence of young cottonwoods on bar/bank edges did not greatly reduce volumes of erosion. The implication of this result for sediment dynamics along the Central Platte River, is that young cottonwoods growing at bar edges do not seem to affect bar edge mobility, and thus sediment delivery to the system. In light of the modeling results and low stem densities of cottonwoods recorded in the field, these young seedlings do not seem to play a significant role in the stabilization of bars and setting up of a positive feedback that leads to bar stabilization, reduced sediment availability within the system, and a shift towards a single thread planform.

5.2 Reed canarygrass

Excavation of Reed canarygrass roots at several locations, and observations of exposed roots at bar and bank edges showed that the root network of this species forms a dense root mat, but that rooting depth rarely extends past 0.5 m. This root mat protects the upper bar or bank surface through mechanical root-reinforcement, and resistance to hydraulic erosion. As the the rooting depth to bank height ratio decreases (i.e. roots protect less of the total bar/bank height), the likelihood of hydraulic scour under the root-reinforced layer increases. In the low cohesion sands and fine gravels that dominate the Central Platte River, this hydraulic erosion can occur either during prolonged low magnitude flows, or during SDHFs. The root mat acts to strengthen the upper layer of bar material, but the BSTEM runs conducted in this study showed that geotechnical failures can occur even under the highest rooting density modeled. Lateral erosion can, therefore, lead to removal of this species at bar and bank edges, where hydraulic scour beneath the root zone is sufficient to tip the balance between driving forces and resisting forces acting on the bar/bank material.

In terms of management implications, the model results presented here suggest that SDHFs, in conjunction with predeeding flow conditions leading to undercutting of the root zone, should then be capable of removing younger stands with shallower root networks. The model results for a SDHF alone showed that when considered in isolation, a 3-day high flow event, was not capable of removing stands of Reed canarygrass. However, extended periods of hydraulic scour, that can occur at lower discharges, can ‘prime’ the bank so that these undercut root zones can be removed during a SDHF event. As with the cottonwood seedlings, as the roots grow to form a denser, deeper mat, it will become increasingly difficult for flows of any magnitude to remove this species. This will be especially true on bars that are lower in height, where the rooting depth to bar/bank height ratio is high. Because Pollen-Bankhead et al. (2010) showed that Reed canarygrass is unlikely to be removed through drag forces acting on the stems, mechanical removal of this species may be necessary where undercutting, and resulting cantilever failures of root-reinforced blocks is unlikely. Reed canarygrass is therefore more likely to stabilize bars, and reduce sediment erosion at bar and bank margins that are low in elevation, where the root zone cannot be undercut as easily

5.3 *Phragmites*

The model results presented in this study showed that with *Phragmites*, little erosion, be it hydraulic or geotechnical, can occur once the rhizomes have grown throughout the depth of the bar or bank, even during SDHFs. This poses more of a problem than cottonwood and Reed canarygrass, both in terms of vegetation management and in terms of sediment dynamics within the braided system of the Central Platte River. The resistance of bank and bar edges to hydraulic and geotechnical erosion that contain stands of *Phragmites*, is likely to promote development of the positive feedback between sediment trapping, bar growth and shifting of the overall planform away from braiding towards that of a deeper, single thread system. The first directed vegetation study showed that this species is very unlikely to be removed through drag forces acting on the stems, even during SDHFs. This study has show that the density and strength of the rhizomes also makes it unlikely that stands of *Phragmites* can be removed through lateral erosion of the bar material. Mechanical removal of the above and below ground biomass of *Phragmites* is likely to be required to remove this species. Spraying of the above-ground biomass may kill the stems and make them more brittle and prone to removal by drag forces at high flows, but the below ground rhizomes can often survive spraying, continuing to protect the bar/bank material from erosion through root-reinforcement even if the above ground biomass is removed.

5.4 Rates of lateral erosion compared to total channel width, and implications for vegetation management

It has been estimated that for a braided system, such as the Central Platte River, to remain free of bar vegetation, lateral bar erosion rates would have to facilitate erosion of half of the main channel width every year or so (Gran and Paola, 2001; Hicks et al., 2008). According to the repeat cross section data, between May and August 2011, erosion at the three bar edges modeled was approximately 5.7 m of (2.5 % of the channel width) at XS2, 17.7 m (5.07% of the channel width) at XS13, and 21.8 m (8.86 % of the channel width) at XS20. The BSTEM results presented here showed that these erosion distances would be reduced further as rooting density and depth increase. These percentages are well below the 50 % value suggested in the literature for maintaining vegetation free bars, even though the flow period bounded by these surveys contained several days above 8,000 ft^3/s, and flows that stayed well above the seasonal average for that time of year. However, these bar erosion widths and associated model results with vegetation only pertain to one bar edge per cross section.

To accurately predict annual lateral retreat over an entire cross section, where multiple bar edges and channels are present, we recommend the use of a 2D flow and sediment transport model. This is because BSTEM Dynamic in its current form, does not take into account the process of deposition, or changing hydraulics as a channel widens, or material is deposited. Traditionally, 2D hydraulic and sediment transport models have assumed fixed banks, so they have also not been able to account for the energy adjustment that occurs as the channels widens. In addition, the assumption of fixed banks means that they fail to account for any hydraulically-controlled sediment coming from these channel banks. However, a new version of the BoR model SRH-2D is currently being tested, that integrates the BSTEM algorithms within the 2D framework, allowing for mobile banks, bars and bed. Use of this model in the Elm Creek Complex for example, would allow PRRIP to compare lateral erosion rates over various flow conditions and vegetation types, ages and densities, by building off of the root data and geotechnical properties collected for this study.

6 Summary and Conclusions

Management of vegetation growing on in-channel bars and at bank edges is a key part of PRRIP's Flow-Sediment-Mechanical (FSM) management strategy for the Central Platte River. An initial study by Pollen-Bankhead et al. (2010) provided results from fieldwork, physical, and numerical modeling, that indicated that out of the three species studied (cottonwood seedlings less than 2-years-old, Reed canarygrass, and *Phragmites*), SDHFs would only be capable of removing the weakest and most shallowly rooted cottonwood seedlings through drag forces acting on the stems. In that report it was suggested that the removal of the same species at bar and bank edges through the interconnected processes of hydraulic erosion and geotechnical failure, should also be investigated as a possible removal mechanism. It was hypothesized that if these species could be removed during SDHF events by lateral erosion, the need for costly and time consuming manual removal of these plants in some locations might be reduced, and would have implications for the sediment balance within the system.

To carry out this study field data were collected to quantify the resistance of the bar and bank materials to hydraulic and geotechnical erosion. In addition, vegetation parameters such as rooting density, diameter distributions and stem densities were measured in the field and added to the data sets already collected in the first study. These field data were used to parameterize BSTEM Dynamic so that the differences between runs with and without various vegetation scenarios could be compared.

Repeat surveys of cross sections corresponding to the three cross sections studied within the Elm Creek Reach, were obtained from PRRIP. At each cross section one bank edge and one bar edge were selected for modeling, and eroded volumes between the two survey dates were calculated at each location. Flow data from the closest USGS gage were input to BSTEM for the May 2011 to August 2011 period between the repeat surveys, and the model was calibrated around Manning's n (to vary applied shear stresses) for the known volumes of erosion between the May and August 2011 surveys. Once the model had been calibrated at each location, the reinforcing effects of vegetation were added, and the model files re-run for a series of scenarios. Mechanical root-reinforcement was accounted for by increasing the effective cohesion of the bank or bar material, and critical shear stress values were increased according to rooting densities measured in the field, to account for the effects of roots on protecting the bar or bank material from hydraulic scour. These vegetation parameters were added to the upper 0.5m of the bar or bank for cottonwood and Reed canarygrass runs, and for the entire bank or bar height for *Phragmites* runs, again based on observations from root excavations performed in the field. The minimum and maximum potential values for root-reinforcement and critical shear stress were used in the model for each species to provide a range of possible erosion volumes over the calibrated period.

The BSTEM runs showed that eroded volumes increased by up to 19% in one of the runs compared to the calibration runs with no vegetation, but that in other runs the addition of roots completely prevented any erosion from occurring (i.e. decreasing erosion by 100 %). The timing and magnitudes of daily eroded volumes by hydraulic and geotechnical processes were controlled not only by the magnitude of reinforcement in the root zone, but also the root zone to bank/bar height ratio. This ratio affected locations and rates of undercutting, and in combination with the various root densities and strengths modeled, produced some complex results. For example, at two of the bar edge locations modeled, more erosion was predicted when Reed canarygrass root densities were at a maximum, than when modeled at minimum values. This result, however, can be misleading as it occurred because the stronger reinforced upper layer in the maximum root density run, allowed more of an undercut to develop before geotechnical failure occurred. Once the gravitational driving forces did overcome the resisting forces, the failure block width was wider, and a large volume of erosion was recorded. In the Reed canarygrass run with minimum root density, the bar edge failed more progressively throughout the run, and the overall eroded volume that resulted was less than the run with maximum rooting density.

Daily erosion totals derived from BSTEM also showed that the low cohesion, sand and silt particles that make up the bars of the Central Platte River, are easily entrained, by hydraulic forces at the channel margins occurring under a wide range of discharges, not just during SDHF events. As a result, a long period of exposure to continual hydraulic erosion still resulted in geotechnical failures of the bar edges under some vegetation scenarios, regardless of the occurrence of a SDHF. This was especially true in the cottonwood runs and to a lesser extent in the Reed canarygrass runs.

Modeling results showed that in general, cottonwood seedlings had the least effect on eroded volumes compared to the calibration run (5 % increase in eroded volume to a 36 % reduction). The Reed canarygrass runs had the most complex results because of the substantial reinforcement of the upper 0.5m layer, combined with a relatively shallow root zone that could be undercut by hydraulic scour (19 % increase in eroded volume to a 47.7 % reduction). In contrast, *Phragmites* had a dramatic effect on eroded volumes compared to the calibration runs (52 to 100 % reduction). In the model runs, lateral erosion of bar and bank edges effectively removed young cottonwood seedlings and areas of Reed canarygrass that could be undercut by hydraulic erosion. The model results for *Phragmites* , however, suggested that its deep rooting network is unlikely to be undercut and the root-reinforcement provided by the interconnected rhizome networks makes resistance to geotechnical failure high. Lateral erosion at bar and bank edges was therefore resisted in most cases by stands of *Phragmites* during both long duration lower flows, or during SDHF events.

The implication for management of cottonwood seedlings in the Central Platte River, is that little intervention to mechanically remove young cottonwoods growing at lower elevations and/or near bar edges. Because lateral erosion was still predicted in the all of the cottonwood model runs, even under the highest root densities modeled, it is likely that those cottonwoods that do survive on bars will be located away from bar edges, and/or at elevations that are subject to shorter durations of hydraulic scour, so that roots have time to establish. Cottonwoods growing at higher bar elevations may, therefore, need to be removed mechanically if their roots become established.

For Reed canarygrass the management implications of the model results are that SDHFs, in conjunction with preceding hydraulic scour of the root zone, should be capable of removing newly establishing stands with shallower root networks, or locations where the rooting depth to bar/bank height ratio is low. As with cottonwood seedlings, as the roots grow to form a denser, deeper mat, it will become increasingly difficult for flows of any magnitude to remove this species. This will be especially true on bars that are lower in height, where the rooting depth to bar/bank height ratio is high. Because Pollen-Bankhead et al. (2010) showed that Reed canarygrass is unlikely to be removed through drag forces acting on the stems, continued mechanical removal of this species may be necessary where undercutting, and resulting cantilever failures of root-reinforced blocks is unlikely.

In terms of vegetation management on channel bars, *Phragmites* poses more of a problem than cottonwood and Reed canarygrass. The model results presented in this study show that with *Phragmites*, little erosion, be it hydraulic or geotechnical, can occur once the rhizomes have grown throughout the depth of the bar or bank, even during SDHFs. The first directed vegetation study also showed that this species is very unlikely to be removed through drag forces acting on the stems, even during SDHFs. Mechanical removal of the above and below ground biomass of *Phragmites* is likely to be required to remove this species.

7 References

Abernethy, B., and Rutherfurd, I.D., 2001. The distribution and strength of riparian tree roots in relation to riverbank reinforcement. *Hydrological Processes*, 15(1), 63-79.

Bagnold, R.A., 1956. Flow of cohesionless grains in fluids. Philosophical Transactions of the Royal Society of London A, 249(964), 235-297.

Bohm, W., 1979. *Methods of Studying Root Systems*. Berlin: Springer-Verlag.

Buffington, J.F., 1999. The legend of A. F. Shields. *Journal of Hydraulic Engineering*, 125(4), 376-387.

Carson, M.A. and Kirkby, M. J., 1972. Hillslope Form and Process. Cambridge

Chow, V.T., 1959. *Open Channel Hydraulics*. McGraw-Hill: New York, NY.

Coppin, N.J., and Richards, I.G., 1990. *Use of Vegetation in Civil Engineering*. Butterworths: London, UK.

De Baets, S., Poesen, J., Gyssels, G., Knapen, A., 2006. Effects of grass roots on the erodibility of topsoils during concentrated flow. Geomorphology 76, 54–67.

De Baets, S., Poesen, J., Galindo-Morales, P., Knapen, A., 2007. Impact of root architecture on the erosion-reducing potential of roots during concentrated flow. Earth Surface Processes and Landforms 23, 1323–1345.

Du Boys, P., 1879. Le Rhône et les Rivières à Lit affouillable. *Annales des Ponts et Chaussées*, 18(5), 141-195.

Einstein, H.A., 1942. Formulas for the Transport of Bed Sediment. Trans. American Society of Civil Engineers, Vol. 107, pp. 561-574

Endo, T., and Tsuruta, T., 1969. *On the effect of tree roots upon the shearing strength of soil*. Annual report of the Hokkaido branch, Forest Place Experimental Station: Sapporo, Japan; pp.167-183.

Ennos, A. R. 1990. The Anchorage of leek Seedlings: The Effect of Root Length and Soil Strength, *Annals of Botany* 65: 409-416.

Fan, C.-C., and Su, C.-F., 2008. Role of roots in the shear strength of root-reinforced soils with high moisture content. *Ecological Engineering*, 33(2), 157-166.

Fredlund, D.G. and Rahardjo, H., 1993. *Soil Mechanics of Unsaturated Soils*. John Wiley and Sons, New York.

Fredlund, D.G., Morgenstern, N.R., and Widger, R.A., 1978. The shear strength of unsaturated soils. *Canadian Geotechnical Journal*. 15, 313-321.

Gran, K. and Paola, C. 2001. Riparian vegetation controls on braided stream dynamics. Water Resources Research, Vol. 37 (12), 3275-3283.

Gray, D.H., and Leiser, A.T., 1982. *Biotechnical Slope Protection and Erosion Control*. Van Nostrand Reinhold Company: New York, NY.

Gray, D.H., and Sotir, R.B., 1996. *Biotechnical and Soil Bioengineering Slope Stabilization: A Practical Guide for Erosion Control.* John Wiley & Sons, Inc.: New York, NY.

Gyssels, G., Poesen, J., 2003. The importance of plant root characteristics in controlling concentrated flow erosion rates. Earth Surface Processes and Landforms 28, 371–384.

Gyssels, G., Poesen, J., Bochet, E., Li, Y., 2005. Impact of plant roots on the resistance of soils to erosion by water: a review. Progress in Physical Geography 29, 189–217.

Hanson, G. J., 1990. *Surface Erodibility of Earthen Channels at High Stresses. Part II - Developing an in-situ testing device. Transactions of the ASAE. Volume 33(1),: 132-137*

Hicks, D.M., Duncan, M.J., Lane, S.N., Tal, M., Westaway, R. 2008. Contemporary morphological change in braided gravel-bed rivers: new developments form field and laboratory studies, with particular reference to the influence of riparian vegetation, In, Habersack, Piegay, Rinaldi, eds, Gravel-Bed Rivers VI: From Process Understanding to River Restoration, Elsevier, p557–581.

Humboldt Manufacturing, 2011. http://www.humboldtmfg.com/manuals/H-4200_Soil_Penetrometer.pdf, accessed December 30, 2011.

Langendoen, E.J., 2000. CONCEPTS – *Conservational channel evolution and pollutant transport system software manual*, USDA-ARS National Sedimentation Laboratory Research Report, 16.

Mamo, M., Bubenzer, G.D., 2001a. Detachment rate, soil erodibility and soil strength as influenced by living plant roots: part II. Field study. American Society of Agricultural Engineers 44, 1175–1181.

Mamo, M., Bubenzer, G.D., 2001b. Detachment rate, soil erodibility and soil strength as influenced by living plant roots: part I. Laboratory study. American Society of Agricultural Engineers 44, 1167–1174.

Morgenstern, N.R., and Price, V.R., 1965. The analysis of the stability of general slip surfaces. *Geotechnique*, 15, 79-93.

O’Brien, M.P. and Rindlaub, B.D., 1934. The transportation of bed-load by streams. *Transactions of the American Geophysical Union*, 15, 593-603.

Partheniades E., 1965. Erosion and deposition of cohesive soils, *Journal of Hydraulic Engineering*, 91(1): 105-139.

Pollen, N., 2007. Temporal and spatial variability in root reinforcement of streambanks: Accounting for soil shear strength and moisture. *Catena*, 69(3), 197-205.

Pollen, N., and Simon, A., 2005. Estimating the mechanical effects of riparian vegetation on streambank stability using a fiber bundle model. *Water Resources Research*, 41, W07025, doi:10.1029/2004WR003801.

Pollen, N., Simon, A., and Collision, A.J.C. 2004. Advances in Assessing the Mechanical and Hydrologic Effects of Riparian Vegetation on Streambank Stability, In: S. Bennett and A. Simon, eds. Riparian Vegetation and Fluvial Geomorphology, *Water Science and Applications* 8, AGU: 125-139.

Pollen-Bankhead, N. and Simon, A. 2009. Enhanced application of root-reinforcement algorithms for bank-stability modeling. *Earth Surface Processes and Landforms*. 34(4):471–480.

Pollen-Bankhead, N., and Simon, A. 2010. Hydrologic and Hydraulic effects of Riparian Root Networks on Streambank Stability: Is Mechanical Root-Reinforcement the Whole Story? *Geomorphology*, 116: 353–362.

Pollen-Bankhead, N., Thomas, R.E., Simon, A. 2010. Can Short Duration High Flows be used to remove vegetation from bars in the Central Platte River. PRRIP Report #. pp.127.

Riestenberg, M., and Sovonick-Dunford, S.S., 1983. The role of woody vegetation in stabilizing slopes in the Cincinnati area. Ohio*, Geological Society of America Bulletin*, 94(4), 506-518.

Schoklitsch, A., 1914. *Über Schleppkraft und Geschiebebewegung*. Engelmann, Leipzig.

Shields, A., 1936. Anwendung der Aechlichkeitsmechanik und der Turbulenz Forschung auf die Geschiebebewegung, *Mitteilungen der Pruessischen Versuchsanstalt fuer Wasserbau and Schiffbau*, Berlin.

Simon, A., and Collison, A.J.C., 2002. Quantifying the mechanical and hydrologic effects of riparian vegetation on stream-bank stability, *Earth Surface Processes and Landforms*, 27(5), 527-546.

Simon, A., Curini, A., Darby, S., and Langendoen, E., 1999. Stream-bank mechanics and the role of bank and near-bank processes in incised channels. *In*: S. Darby and A. Simon, eds. Incised River Channels. John Wiley and Sons, New York, 123-152.

Simon, A., Thomas, R.E., and Klimetz, L., 2010. *Comparison and experiences with field techniques to measure critical shear stress and erodibility of cohesive deposits*. Federal Interagency Sedimentation Conference, Las Vegas, NV, 2010, 11 p. (on CD).

Simon, A., Pollen-Bankhead, N. and Thomas, R.E., 2011. Development and Application of a Deterministic Bank Stability and Toe Erosion Model for Stream Restoration. In: Simon, A., S.J. Bennett, J. Castro and C.R. Thorne (eds.), Stream Restoration in Dynamic Systems: Scientific Approaches, Analyses, and Tools. American Geophysical Union: Washington.

Simon, A., Wolfe, W. J. and Molinas, A., 1991. Mass Wasting Algorithms in an Alluvial Channel Model. Proceedings of the 5th Federal Interagency Sedimentation Conference. Las Vegas, NV. Volume 2, 8-22 to 8-29 p.

Temple, D.M., 1980. Tractive force design of vegetated channels. *Transactions of the American Society of Agricultural Engineers*, 23(4), 884-890.

Temple, D.M., Robinson, K.M., Ahring, R.M., and Davis, A.G., 1987. *Stability Design of Grass-Lined Open Channels*. USDA ARS Agriculture Handbook Number 667. US Government Printing Office: Washington, DC.

Thorne, C.R., 1990. Effects of vegetation on riverbank erosion and stability, In: J.B. Thornes, (ed.), *Vegetation and Erosion*. John Wiley & Sons Ltd.: Chichester, UK; pp.125-144.

Thorne, C.R., 1982. Processes and Mechanisms of River Bank Erosion. In, Hey, R.D., Bathurst, J.C. and Thorne, C.R., (Eds.). Gravel-Bed Rivers, John Wiley and Sons, Chichester, England. 227-271 p.

Thorne C.R, and Tovey N.K., 1981. Stability of composite river banks. *Earth Surface Processes and Landforms* 6: 469- 484

van Genuchten, M. Th., 1980. A closed-form equation for predicting the hydraulic conductivity of unsaturated soils. Soil Science Society of America Journal, 44, 892-898.

van Rijn, L.C., 1984. Sediment transport, Part I: Bed load transport. *Journal of Hydraulic Engineering*, ASCE, 110(10), 1431-1456.

Waldron, L.J., 1977. The shear resistance of root-permeated homogeneous and stratified soil. *Soil Science Society of America Journal*, 41(5), 843-849.

Waldron, L.J. and Dakessian, S. 1981. Soil Reinforcement by Roots: Calculation of increased soil shear resistance from root properties, *Soil Science* 132: 427-435.

Wu, T.H., 1984. Effect of vegetation on slope stability, *Transportation Research Record*, 965, 37-46.

Wu, T.H., McKinnell, W.P. III, and Swanston, D.N. 1979. Strength of tree roots and landslides on Prince of Wales Island, Alaska, *Canadian Geotechnical Journal* 16**:** 19-33.

Wu, W., Wang, S.S.Y., and Jia, Y., 2000. Nonuniform Sediment Transport in Alluvial Rivers. *Journal of Hydraulic Research,* 38(6), 427-434.